UNIVERSITY OF BUCHAREST
FACULTY OF PHYSICS

NANOSTRUCTURED THIN FILMS SYNTHESISED BY ADVANCED LASER TECHNIQUES FOR RAPID HEALING AND TISSUE REGENERATION

PhD thesis summary

Anita Ioana GHIȚĂ (VIȘAN)

Scientific coordinator: Prof. Dr. Ion N. MIHĂILESCU

Bucharest, 2015

Table of contents

CHAPTER 1. INTRODUCTION

The PhD project was dedicated to nanostructured thin films fabrication by advanced laser techniques with antimicrobial properties for rapid healing and bone regeneration. The thesis report the synthesis and characterization of three types of bioactive implants with antimicrobial properties based on hydroxyapatite (HA)deposited on simple titanium substrate and functionalized substrate with titanium dioxide nanotubes.

In this thesis are discussed two laser techniques for coating and functionalization of implants: Pulsed Laser Deposition (PLD) and Matrix-Assisted Pulsed Laser Evaporation (MAPLE), respectively. The interconnections between the implemented approaches and studied biomaterials are described in Figure 1.

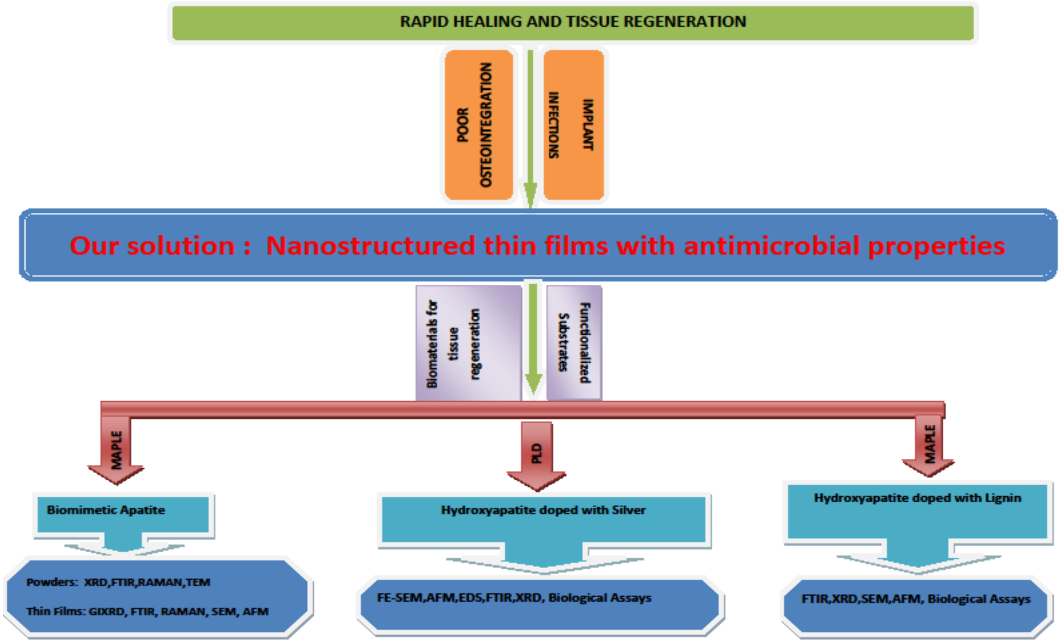

Fig. 1. A flowchart over the correlations between implemented approaches and studied biomaterials

Thesis Organization

Studies on bioactive coatings obtaining synthesis by PLD and MAPLE with antimicrobial properties were initiated in the National Institute for Laser, Plasma and Radiation (INFLPR) in Lasers Department, “Laser-Surface Plasma Interactions” Laboratory (LSPI) Romania, but also in collaboration with the Faculty of Technology and Metallurgy, University of Belgrade, Serbia and Laboratory CIRIMAT, Ensiacet, Toulouse, France. After identifying the optimal experimental parameters for each biomaterial deposition, thin films obtained were analyzed in terms of physical, chemical and especially biological behavior. Through collaboration with specialized institutes were performed cell culture analyzes and antimicrobial tests to assess the performance of biofunctional implants and to ensure the structural integrity of bone reconstruction.

The thesis is divided into five chapters:

(i) Chapter 1: "Introduction" is devoted to the current state-of-art of the research and thesis organization

(ii) Chapter 2: "Biomaterials investigated in the thesis" describes the properties and applications of biomaterials used in the experimental research. In order to achieve this purpose we approached three types of materials:

- *Biomimetic apatite (BmAp).* As known, the actual composition of apatites that are present in human bone is Ca deficient, but contains many other ions and trace elements. In this context, new materials are introduced. The BmAp obtained by the co -precipitation method is composed of nanocrystals similar to those present in human bone. An key factor is the synthesis temperature and working at low temperature allows to keep the size of nanocrystals in a reasonable range. This approach along with other conditions constitutes the originality of biopowders synthesis method used in this work.
- *Hydroxyapatite doped with silver (Ag:HA).* Hybrid nanostructured films with antibacterial properties against *C. albicans* and *A Niger* were obtained. In the thesis was found the most appropriate concentration of Ag in the HA ensuring at the same time the maximum antimicrobial activity and the absence of any toxic effect on growth of mezemchimal cells. We mention that these cells are the ones of the tissues surrounding the coated metal implant.
- *Hydroxyapatite doped with lignin (Ag-Lig:HA).* Were synthesized thin films with antimicrobial activity with the aim to find solutions to combat pathogens without resorting to antibiotics

(iii) Chapter 3 "Methods and equipment used for the synthesis and characterization of nanostructured thin films" illustrates methods of obtaining and optimized operating modes to achieve metallic implants developed. Were described the principal elements of the of pulsed laser deposition methods, their advantages and set-ups. It also briefly lists for each case, the methods and characterization of thin films obtained.

(iv) Chapter 4 "Results and discussion" is the core work and contains original contributions in the field of laser interactions and their applications. It discusses all compositions of biomimetic apatite, hydroxyapatite doped with silver and lignin, respectively. In the first case, the intended purpose was to obtain thin layers as close to the composition, structure and morphology of human bone. In the other two cases, we referred to doped hydroxyapatite with inorganic (Ag) and organic (Lignin) materials with proven therapeutic action, effectively combating germs. It should be noted that the research covers a wide range of apatite compounds and is addresses to a very hot issue, ensuring a stable and active protection against contamination with bacteria and fungi. There are presented and analyzed the main results and characteristics of the obtained structures and their correlation with experimental conditions for each case;

(v) In Chapter 5 "Conclusions and Perspectives" it is included the summary of the original contributions and results of the work.

At the end of the thesis it can be found references and copies of relevant articles published by the author.

CHAPTER 2. Biomaterials investigated in thesis

Calcium phosphate (CaP) ceramics are currently used for metal implant coating in order to increase the osseoconductivity and overall bioactivity, thus speeding up the biointegration and repairing process of bones or other hard tissues [1]. Nevertheless, recent studies have shown that the actual bioapatite present in the human body is generally nonstoichiometric and much more soluble than pure hydroxyapatite [HA, $Ca_{10}(PO_4)_6(OH)_2$], which is considered the model for the basic constituent of the inorganic part of the bone (65-75 wt. %, depending on age and sex) [2, 3].

The first study has been therefore concentrated on the synthesis of bioapatite materials as close as possible to the human bone composition and structure, and their next congruent transfer onto the surface of metallic implants [4, 5].

In this context the apatite nanocrystals obtained by precipitation methods in solution present physico-chemical features similar to those of bone nanocrystals, which make them very promising biomaterials for the preparation of highly bioactive ceramics [6]. Non-stoichiometric nanocrystalline apatite-based biomaterials mimic the mineral bone crystal structure and composition and exhibit a controlled reactivity in respect to the interactions with components of biological fluids (ions, proteins) [7]. Recently, apatite nanocrystals have been tested as coatings and they have shown superior biological behaviour [8]. One significant property is their surface reactivity that is related to the existence of a metastable hydrated layer on the surface of the nanocrystals in powders [2]. The synthesis process of nanocrystalline apatites poorly crystallized by conventional techniques, at high temperature, strongly alters their physico-chemical characteristics and biological properties. The synthesis processes used in this paper were therefore aimed to limit these alterations (as grain growth, dehydration, evolution toward stoichiometry) [9].

We underline the advantages for processing the powders at low temperature and illustrated the effect of experimental parameters' synthesis on apatite powder characteristics. The non-stoichiometric nanocrystalline apatite bioceramic coatings were deposited on titanium (Ti) substrates by Matrix-Assisted Pulsed Laser Evaporation (MAPLE) technique, considered the most convenient for the well–protective transfer of novel organic delicate molecules thin films [10, 11]. MAPLE ensures good thickness control, patterning facility, and is appropriate for a wide range of biomaterials prone to the decomposition and/degradation under direct intense laser irradiation and subsequent exposure to plasma action [10-12]. One can deposit patterned films on a variety of substrate materials with different geometric shapes. The most important requirement of MAPLE process is to minimize and possibly avoid the photonic damage, either of the film or of matrix material during laser interaction and transfer [10-12]. MAPLE is a non-contact deposition technique, which eliminates major sources of contamination and can be integrated with other sterile processes [10-12].

As a metal substrate for regenerative medicine applications, such as orthopedic or dental implants, titanium (Ti) is widely preferred due to its desirable properties, such as suitable elastic modulus and mass density, good mechanical strength, corrosion resistance, biocompatibility and low toxicity [13,14-16]. However, Ti exhibits a rather poor bioactivity and in order to establish a direct chemical bonding between the implant and the host bone tissue its adequate surface modification was suggested using various routes [17].

In our second study of the thesis project we propose an approach to enhance the bioactivity and improve the bone response to implant surface is by depositing bioactive HA thin films on Ti implant surface.

Recently, nanotubular titanium dioxide (TiO_2) layers have attracted an increased attention in comparison to pure Ti due to their ability to enhance the bonding strength between HA coating and metallic substrate [18-20]. The nanotubes fabrication by electrochemical anodic oxidation of pure Ti in fluoride-containing electrolytes provides strongly adherent layers which are used for various applications, based upon their semiconductive and biocompatible nature [20].

A challenging task in biomedicine is the prevention of microbial infections which determine the loosening of implants from the bone [13,21]. A promising strategy to prevent the initial microbial adhesion and colonization of biofilms is via introducing antimicrobial bioactive thin films onto implant's surface. Some previous studies have shown that Ag^+ ions have a broad spectrum of antimicrobial and antifungal properties [22] while maintaining a low cytotoxicity [23]. The Ag^+ ions are able to penetrate the microbial cell wall and bind to DNA, and thus interfering with the replication process [24-26]. Currently, special interest is focused on the development of HA coatings doped with silver to minimize microbes' adhesion [27].

There are various methods to deposit ceramic thin films on metal surfaces, such as plasma spraying [28], magnetron sputtering [29], pulsed laser deposition [30,31], sol−gel [32], electrochemical or electrophoretic deposition [33-35]. Pulsed laser deposition (PLD) is a technique that has proved efficient in the fabrication of calcium phosphate films on metallic substrates with excellent coating attachment [30]. Moreover, by a proper choice of the ablation and deposition parameters, it is possible to control the stoichiometry and crystallinity of a wide range of complex materials deposited at room temperature (RT) [13,30].

In the second study we report on the physical-chemical characterization of HA and Ag doped HA [$Ca_{9.95}Ag_{0.05}(PO_4)_6(OH)_2$] thin films with Ag content of (0.53 ± 0.1) wt. %, synthesized by PLD on pure Ti and Ti modified by TiO_2 nanotubes substrates. The antifungal efficiency of the novel Ag:HA/TiO_2 nanotubes structures was tested against two pathogenic, largely spread, fungal strains: *Candida albicans* and *Aspergillus niger*. The specific aim of this manuscript is the identification of the most suitable deposition substrates and optimal processing conditions.

Recent research advances in understanding the interaction between microbial biofilms and Ti surface contributed to the development of novel preventive strategies to control medical device-related infections. The focus is on obtaining improved biomaterials with increased resistance to microbial colonization via surface physical-chemical modifications.

Lignin (Lig) is a complex, amorphous organic polymer found in plant tissues, usually bound to cellulose. Phenylpropane units in Lig are cross-linked to each other by various chemical bonds. Lig is a well-known and important source of natural antimicrobial and antifungal compounds [36].

The novel concept of engaging natural biopolymer Lig in composite coatings was studied so far by electrophoretic deposition only [37,38]. However, an unaltered incorporation of this specific organic material could provide a composite with enhanced stability and improved interconnected structure, which will increase the coating cohesion.

In the second study we have demonstrated the positive role of the Ti surface modification by arrays of TiO_2 nanotubes on the biocompatible and antifungal response of top HA layers deposited by PLD [39]. In the third study, we aimed to obtain biomimetic ceramic-polymer composite coatings for medical Ti implants modified with 100 nm diameter TiO_2 nanotubes (fabricated by anodization of Ti plates) by employing MAPLE as fabrication method. Composite HA-Lig and Ag doped HA-Lig were transferred by this technique, their structure and composition were assessed, as well as their cytotoxicity against human Wharton's Jelly-derived mesenchymal stromal cells (WJ-MSCs) and antimicrobial efficiency against Gram-positive (*S. aureus* ATCC 6533), Gram-negative (*P. aeruginosa* ATCC 27853) bacterial and fungal (*C. famata* 30) strains.

The purpose of this work was to evaluate the anti-biofilm efficiency of thin films of simple hydroxyapatite (HA) or silver (Ag) doped HA combined with the natural biopolymer organosolv lignin (Lig) (Ag-Lig:HA), deposited by MAPLE.

CHAPTER 3. Materials and methods

3.1. Study I: Biomimetic Apatite

3.1.1. Synthesis of biomimetic apatite powders

Biomimetic Apatites (BmAp), with complex chemical formula $Ca_{10-x+u}(PO_4)_{6-x-y}(HPO_4^{2-})_{x+y}(OH)_{2-x+2u+y}$, $0\leq x\leq 2$ and $0\leq 2u+y\leq x$ [40], were synthesized at room temperature (RT) and physiological pH by double decomposition method between a phosphate and a carbonate solution [120 g of $(NH_4)_2HPO_4$ in 1500 ml of deionised water, 52.2 g of $Ca(NO_3)_2 4H_2O$ in 750 ml of deionised water]. The calcium solution was rapidly poured into the phosphate solution at 20 ^{o} C and stirred for a few minutes. After maturation for one day, the precipitates were filtered under vacuum and washed with deionised water. Then, the gel was freeze-dried and finally stored in a freezer to prevent further maturation of the BmAp nanocrystals. The chosen conditions (physiological pH of 7.4 in close resemblance to human body, with large excess of phosphate) resulted in the synthesis of a poorly crystalline apatite analogous to mineral neo-formed bone.

3.1.2. Thin films deposition of BmAp

The MAPLE set-up used in experiments is depicted schematically in Figure 2.

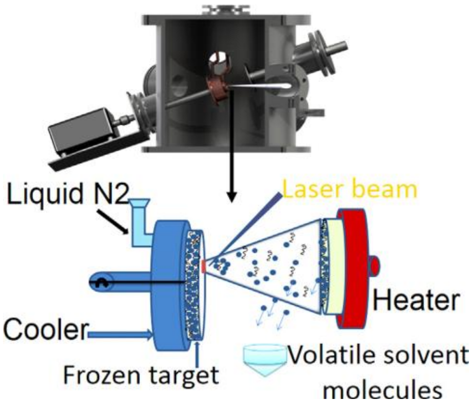

Fig. 2. MAPLE experimental set-up

Thin BmAp films have been deposited using a KrF* excimer laser source ($\lambda = 248$ nm, $\tau_{FWHM} \leq 25$ ns), running at a repetition rate of 10 Hz.

The most used substrates for the experiments were disks of pure titanium (Ti) of 1.2 cm in diameter and 0.2 cm in thickness. For microscopic characterizations, some structures were deposited on <110> single-crystalline Si wafers. All substrates were degreased in acetone and ethanol in an ultrasonic bath for 30 min and rinsed with deionized water. For MAPLE experiments, the slurry was prepared by dispersing a few grams of BmAp, maturated for one day, in a hydro alcoholic solution, where benzoic acid was previously dissolved. The resulting slurry was carefully stirred at RT and then poured in a stainless steel cup. The solution was next frozen at 77 K by immersion in liquid nitrogen in direct contact with a cooler inside the deposition chamber. This way, the target evaporation was slowed down and even stopped. The target-substrate separation distance was of 5 cm. During deposition, the targets were rotated with 0.3 Hz and translated along two orthogonal axes to avoid piercing and to ensure the deposition of a uniform film.

The residual working pressure inside the deposition chamber was set at 2,67 Pa ($2x10^{-2}$ torr). For the deposition of each film, 30000 subsequent laser pulses have been applied.

The selected volatile solvent, the benzoic acid, is highly absorbing the laser wavelength in frozen state, but is not reacting with the solute even under laser exposure. According to literature, the dehydration effect of BmAp after the suspension of powder in a hydro alcoholic solution keeps negligible [41]. The pulsed laser intensity was adjusted in order to prevent the BmAp decomposition. After optimization, the laser fluence was therefore set at 0.75 J/cm^2 in all experiments. This way, the structural and functional fidelity was preserved after MAPLE transfer, by avoiding a significant direct laser–biomaterial interaction in the deposition chamber. Due to the low concentration of solute (biomaterial) in the frozen target, the laser photons preponderantly interact with the matrix (solvent), which is vaporized [42]. The metastable BmAp molecules are released unaltered and, by means of collisions with the other molecules, are directed toward the substrate, where they form a uniform thin film. In the same time, the volatile solvent is pumped away by the vacuum system.

3.2. Study II: Ag:HA

3.2.1. Preparation of Ti modified by TiO_2 nanotubes

Ti plates of (20x10x0.25) mm^3 (99.7% purity, Sigma Aldrich) were used as substrates for the growth of nanotubes titanium oxide film. The substrates were degreased in acetone and ethanol in an ultrasonic bath for 30 min and rinsed with deionized water. The anodization was performed under constant mixing in a two-electrode cell. The Ti plate was the working electrode and a Pt plate was used as a counter electrode at a distance of 15 mm in 0.4 wt. % HF solution. The experiments were carried out by PEQLAB Power Supply EV231 and performed potentiostatically (20 V for 30 min) at RT. After anodization, the samples were rinsed with deionized water and air dried at RT. Prior to PLD experiments, the anodized Ti plates were thermally treated by using a ULVAC-RIKO MILA-5000 instrument at 450 °C for one hour, in air with a heating/cooling rate of 30 °C/min.

3.2.2. PLD experiment

PLD targets (20 mm diameter) were prepared by pressing HA and Ag:HA (0.53 ± 0.1 wt. %) nanopowders at 3 MPa and sintering at 650 °C for six hours. The heating/cooling rate was set at 25/15 °C/min. Our option for Ag doping concentration was based upon the results we reported in Ref. 31. As reported in Ref. [31], we cultivated mesenchymal stem cells on compositional library of Ag and HA layers. It was shown that an Ag content of up to 0.6 wt. % into HA deposited by PLD could be considered nontoxic for cells. Accordingly, we have selected an Ag concentration of 0.53 ± 0.1 wt. % as the best compromise between the highest possible antimicrobial activity and absence of toxic reaction regarding cell removal or apoptosis, in the case of PLD films.

PLD was performed inside a stainless steel deposition chamber. The deposition of the HA and Ag:HA thin films was conducted by ablation of respective targets with a KrF* excimer laser source ($\lambda = 248$ nm, $\zeta_{FWHM} \leq 25$ ns). The repetition rate was of 10 Hz and the applied fluence was set at 4.5 J/cm^2 (with corresponding laser energy of 435 mJ). For the deposition of each film, 15000 subsequent laser pulses have been applied. During the multipulse laser irradiation process, the targets were rotated with 0.4 Hz and translated along two orthogonal axes to avoid drilling and to ensure the deposition of an uniform film.

The films were deposited at 50 Pa in water vapors flux on Ti or anodized Ti substrates that were heated at 500 °C. For some analyses, twin samples were deposited on <111> single-crystalline Si wafers. A target-to-substrate distance of 50 mm was used in all experiments. In order to explore the effect of the post-deposition treatment in restoring the stoichiometry and improving the crystallinity of the thin films, half of the samples were submitted to a post-deposition thermal treatement for six hours at 500 °C in a water vapors enriched atmosphere. The heating/cooling rate in this case was 20/10 °C/min. Depending on the top apatite layer and substrate nature the samples will be further denoted as *HA/Ti* (HA deposited on Ti substrate), *HA/n*TiO_2*/Ti* (HA deposited on Ti modified by TiO_2 nanotubes), *Ag:HA/Ti* (silver doped HA deposited on Ti substrate) and *Ag:HA/n*TiO_2*/Ti* (silver doped HA deposited on Ti modified by TiO_2 nanotubes), respectively.

3.3. Study III: Ag-Lig:HA

3.3.1 Preparation of Ti substrata

Pure Ti foils (20x10x0.25) mm^3 in size and 99.7% purity (Sigma Aldrich) were used as substrata for the growth of arrays of TiO_2 nanotubes by anodization technique described in Ref. 30. As prepared, TiO_2/Ti substrata were degreased in acetone, then in ethanol, each for 30 min in ultrasonic bath and finally kept in ethanol until deposition. Just before their introduction into the reaction chamber, the substrata were rinsed with deionized water and jet-dried with N_2.

3.3.2 Preparation of HA and Ag/HA powders

For the preparation of HA powder with and without Ag we used a modified chemical precipitation method [43]. Calcium oxide, synthesized by aerobic calcination of $CaCO_3$ for 5h at 1000°C, was placed in a reaction vessel with Ag nitrate ($AgNO_3$), in the case of Ag:HA, and phosphoric acid. The reaction was conducted in a step-wise manner. A stoichiometric amount of the resulting calcium oxide was mixed and stirred in distilled water for 10 min. Afterwards, $AgNO_3$ solution was added to the suspension, to reach a final concentration of Ag ion of (0.6 ± 0.1) wt. %. Finally, phosphoric acid was added drop-wise to the suspension in order to obtain HA or Ag/HA powder, $Ca_{9.95}Ag_{0.05}(PO_4)_6(OH)_2$. After the required quantity of phosphoric acid was introduced, the pH reached a value of 7.4−7.6. The obtained suspension was preheated to (94 ± 1)°C for 30 min and stirred for another 30 min. After sedimentation, the upper clear solution layer was decanted from precipitate. The suspension was then spray-dried at (120 ± 5)°C into granulated powder.

3.3.3 Cryogenic target preparation and mounting

Organosolv lignin (extracted by the Alcell process) was used for preparing organic-inorganic composite targets.

Solutions consisting of HA or Ag:HA powders (10% w/v) and Lig (1% w/v) dissolved in distilled water were homogenized by rapid vortexing and flash frozen in a liquid nitrogen cooled copper container. The container with the obtained frozen target (HA-Lig or Ag:HA-Lig pastilles) was then mounted on a cryogenic holder inside the deposition chamber and rotated at 10 rpm to avoid local overheating and excess ablation during multipulse laser irradiation. The holder was submerged in liquid nitrogen flow in order to keep the targets frozen during the experiments

3.3.4 MAPLE experiment

HA-Lig and Ag-Lig:HA composite coatings deposition was performed at room temperature in a pressure of 6.5 Pa onto TiO_2/Ti substrata. The target-to-substratum separation distance was 35 mm. A pulsed KrF* excimer laser source ($\lambda = 248$ nm, $\tau_{FWHM} \leq 25$ ns) operating at 10 Hz was used for target evaporation. The laser beam was incident onto the target surface at 45°. The spot size was of 25 mm^2. A total of 35000 pulses with an incident laser fluence of 0.7 Jcm^{-2} were applied for the deposition of each structure. It is important to note that this fluence level is about five times lower than in conventional PLD of inorganic materials, as a supplementary precaution adopted in MAPLE to protect Lig molecules against extensive laser beam irradiation. Twin samples were deposited on <111> single-crystalline Si wafers.

3.4. Characterization Methods

3.4.1. Study I: Biomimetic Apatite

3.4.1.1. Nanopowders' investigation

All the chemical analysis methods used for apatite characterization were based on the dissolution of apatite in acidic solution before the analysis, for the calcium and orthophosphate ions control, or during the analysis, in the case of carbonate ions, respectively.

Calcium concentration in the initial powders was measured by atomic absorption spectroscopy, using a PerkinElmer AAnalyst 300 Atomic Absorption Spectrometer. The phosphorus concentration was determined by spectrophotometry of the phospho-vanado molybdenum complex, using a Hitachi V-1100 Spectrophotometer at 460 nm, respecting the protocol described in Ref 44.

The sample characterization by X-ray diffraction (XRD) was performed using a curved counter diffractometer INEL CPS 120 with monochromatic Co K_{α} radiation ($\lambda = 1.789$ Å). We mention that Co radiation was currently used for calcium phosphate materials in order to highlight impurities or secondary phases with high cell parameters.

Fourier Transform InfraRed (FTIR) Spectroscopy analysis was carried out on a Perkin Elmer 1600 °C thermo-spectrometer with a resolution of 4 cm^{-1}, for both powders and thin films.

The Raman spectra of powders and thin films were recorded on a Jobin Yvon HR 800 spectrometer, in the (3800-100) cm^{-1} range, with a laser excitation wavelength of 632.8 nm.

Transmission Electron Microscopy (TEM) studies were conducted on a JEOL JEM 1011 (100 kV – 500 kV) microscope.

3.4.1.2.Thin Film studies

Thin film thickness was measured with a Stylus Profiler XP- 2 system (Ambios) of 0.1 nm vertical resolution, an optical deflection height-measurement sensor and stylus with 2.5 μm radius and 0.1 mg force.

FTIR and Raman spectra were recorded on the same systems used for nanopowder characterisation.

The morphology of the surface was examined by Scanning Electron Microscopy (SEM), using a XL-30-ESEM TMP microscope. Additionally, Atomic Force Microscopy (AFM) tests were performed. Microscopic studies were carried out with an AFM Agilent 5500 equipped with a supersharp TESP-SS Nanoworld tip (nominal resonance frequency 320 kHz and nominal radius curvature 2 nm).

3.4.2. Study II: Ag-HA

3.4.2.1. Physical-chemical characterization of deposited films

The surface morphology of the deposited films was investigated by field emission scanning electron microscopy (FE-SEM) with a FEI Inspect S electron microscope. The investigations were performed at 20 kV acceleration voltage, in high vacuum, under secondary electrons acquisition mode. The samples were coated with a thin Au film in order to prevent electrical charging. Cross-section SEM images were recorded on HA and Ag:HA thin films deposited on Si wafers in order to evaluate the thickness. Compositional energy dispersive spectroscopy (EDS) analyses were performed with a SiLi type detector (model EDAX Inc.), operated at 20 kV. The EDS analyses were conducted in duplicate on film regions having areas of (250×250) μm^2. Both sets of experiments lead to comparable results and for that reason, only results from one of the two quantitative analyses are presented in the paper. The thin films roughness was examined by atomic force microscope (AFM), using a Nanonics Multiview 4000 apparatus in tapping mode with a feedback phase.

Fourier transform infrared (FTIR) spectroscopy study was conducted with a Perkin Elmer BX Spectrum spectrometer, in attenuated total reflection mode, using a Pike-MIRacle diamond head of 1.8 mm diameter. The spectra were recorded in the range of (4000 – 550) cm^{-1}, with a resolution of 4 cm^{-1} and a total of 50 scans/experiment.

Identification of crystalline phases in the PLD thin films was carried out by X-ray diffraction (XRD) in symmetric geometry, using a Bruker D8 advance diffractometer, with Cu K_α (λ=1.5418Å) radiation. The diffractometer is equipped with a high efficiency one-dimensional detector (Lynx Eye type) operated in integration mode. The scattered intensity was scanned in the 2θ range (20–60)°, with a step size of 0.04°, and 10 s/step.\

3.4.2. 2 Cytotoxicity assay

A *Hep2* cell line (ATCC® CCL-23™) was was used to assess the cytocompatibility of the PLD films in terms of cellular adhesion, viability and proliferation. Dulbecco's Modified Eagle Medium: Nutrient Mixture F-12 (DMEM:F12) (Sigma, USA) supplemented with 10% fetal bovine serum (FBS) was used as cell culture medium. Prior to biological testing each material (glass control, Ti-control, $nTiO_2$/Ti-control, and Ag:HA/$nTiO_2$/Ti) was sterilized for 1 h at 180 °C in dry atmosphere. Cells were harvested from the substrate using a trypsin:EDTA treatment and brought to a density of 1.5 x 10^5 cells/ mL in DMEM:F12 medium supplemented with 10% FBS. Further, the cell suspension was placed on biomaterial surfaces and allowed to grow for 48 h at 37 °C in a 5%CO_2 humid atmosphere.

The adherence of the cells to materials and cells viability were evaluated using fluorescein diacetate (10 µg/mL) and propidium iodide (10 µg/mL) stain, and their fluorescence was quantified with an Observer.D1 Carl Zeiss microscope.

After 48 the cells were harvested from the sample surfaces, washed in a cold phosphate buffered saline (PBS) solution (pH=7.5), and then fixed overnight in 70% ethanol at –20 °C. The samples were washed with PBS, treated with RNAse A (1 mg/mL) and labelled with propidium iodide (100 µg/mL) at 37 °C for 1 hour. Then, the DNA content of cells was quantified on a Beckman Coulter EPICS XL flow cytometer and analysed by FlowJo 8.8.6 software (Ashland, Oregon, USA).

3.4.2.3. Assessment of antifungal activity

The antifungal efficiency of the deposited thin films was tested according to ASTM E2180 – 07 (2012) standard. This method can be used to evaluate effectiveness of incorporated/bound antimicrobials in hydrophobic materials. The aqueous based microbial inoculum remains in close, uniform contact in a “pseudo-biofilm” state with investigated material. The percent reduction in the surviving populations of microbial cells at 24 hours *vs.* those recovered from the control was determined.

The colony plate count method was used for quantifying the antifungal effect. The test was applied to two sets of specimens: *Candida albicans* (ATTC 10231) and *Aspergillus niger* (IMI 45551). *Candida albicans* is the most common fungus that causes the infection by adhesion onto implant surfaces leading to biofilms formation. It is therefore considered a dangerous pathogenic microorganism [45]. *Aspergillus niger* is usually causing the formation of so called “black mold”. The spores are especially dangerous when inhaled. Moreover, these fungal colonies can be found in ventilation ducts in health care facilities [46].

The solvent for the inoculum was an Agar slurry which reduces the surface tension and allows for the formation of a “pseudo-biofilm”, providing an even contact with the test surface. Decimal dilutions were prepared in sterile physiological saline buffer (0.877 % w/v, pH 7.2) until a final dilution of 10^{-3} and a concentration of 3.9×10^5 CFU/mL for *Candida albicans* and of 7.4×10^5 CFU/mL for *Aspergillus niger*.

The samples were incubated along with the inoculum for 24 hours at a temperature of 37 °C for *Candida albicans*, and 29 °C for *Aspergillus niger*. After incubation, the samples were washed with sterile physiological saline buffer and the cells were passed on Petri plates with Sabouraud, Dextrose-Agar growth media for *Candida albicans* and Czapek-Dox media, for the *Aspergillus niger*. Next, the colonies were counted, and the results were expressed as percentage reduction rate. All samples were tested in triplicate.

3.4.3. Study III: Ag- Lig:HA

3.4.3.1. Morphological, structural and compositional characterization

The surface morphology of the deposited films was investigated by Scanning Electron Microscopy (SEM) with a *Carl Zeiss EVO 50 XVP* instrument, operated at 30 kV acceleration voltage and 10 µA beam current, under secondary electron mode. No conductive coating was applied onto film surface. Cross-sectional SEM images were recorded on HA-Lig and Ag:HA-Lig films deposited on Si wafers in order to evaluate their thickness.

Composition analysis was performed by Energy Dispersive Spectroscopy (EDS), with a *SiLi EDAX Inc.* detector, operated at 20 kV. The measurements were conducted in duplicate, on different, relatively large regions of $(250 \times 250)\ \mu m^2$.

The crystalline status of the MAPLE thin films was evaluated by Grazing Incidence X-Ray Diffraction (GIXRD) using a *Bruker D8 Advance diffractometer,* in parallel beam setting, equipped with a Cu target X-ray tube. The incidence angle was set at 2°, and the scattered intensity was scanned in the range 20–50° (2θ), with a step size of 0.04°, and 50 seconds per step.

X-ray Photoelectron Spectroscopy (XPS) analysis was performed to assess the Lig transfer. The XPS measurements were conducted in a *SPECS* dedicated surface science facility, keeping the base pressure during measurements below 10^{-8} Pa. The spectra were recorded using the Al $K_{\alpha 1}$ monochromatized radiation (E=1486.74 eV) in an analysis chamber equipped with a 150 mm hemispherical electron energy analyzer (Phoibos). Fixed analyzer transmission mode was operated with pass energy of 20 eV and step energy of 0.05 eV. The estimated combined (source+analyzer) resolution was about (0.75±0.025) eV. During the XPS measurements, a flood gun operating at 1 eV acceleration energy and 100 μA electron current was used in order to achieve sample neutralization.

The short-range order analysis and the detection of the functional groups present in the MAPLE films was carried out by Fourier Transform Infra-Red (FTIR) Spectroscopy in Attenuated Total Reflection (ATR) mode using a *Perkin Elmer BX Spectrum-Pike* spectrometer equipped with a *Pike-MIRacle* ATR diamond head of 1.8 mm in diameter. The spectra were collected over a range of (4000–550) cm^{-1} by recording 150 individual scans at 4 cm^{-1} resolution. During acquisition, the spectrometer chamber was continuously purged with nitrogen to maintain a dry environment.

3.4.3.2. Biological assays

3.4.3.2.1. Cytotoxicity assay

The biological compatibility of the MAPLE composite coatings was assessed by cultivating human Wharton's Jelly-derived Mesenchymal Stromal Cells (WJ-MSCs) on their surface. Quantification of cells was performed using propidium iodide (PI). To this purpose, the obtained specimens were sterilized by UV irradiation and placed in 35 mm diameter Petri dishes. In each Petri dish $3x10^5$ mesenchymal cells were added. The monolayer morphology was evaluated after 24h, by fixing the cells with 70% alcohol and staining the monolayer with 5 μg/mL PI. The stained specimens have been examined and photographed in fluorescent microscopy [47].

3.4.3.2.2. Microbial biofilm assay

The microbial adherence ability and biofilm development on the functionalized surfaces have been investigated by two culture-based methods, using Gram-positive (*S. aureus* ATCC 6533), Gram-negative (*P. aeruginosa* ATCC 27853) bacterial and fungal (*C. famata* 30) strains. The specimens (composite coatings and pure HA controls) of the same size have been distributed in the multi-well plastic plates, and exposed to UV sterilization for 30 min. The pure HA controls have been synthesized by PLD in optimized conditions [30]. All experiments were performed in duplicate. Thereafter, the liquid culture medium (nutrient broth) was added over the slide specimens. Each well was inoculated with a microbial inoculum with a density corresponding to 0.5 MacFarland density prepared in sterile saline. Each microbial strain was inoculated in two wells containing the same specimen. Thus prepared samples were incubated at 37°C, in order to allow microbial strains to multiply and adhere to the deposited Ti plates, distributed in each well.

After 24h, 48h and 72h, respectively, the specimens were extracted, washed three times in sterile saline, in order to remove the non-adherent bacteria and moved in sterile plastic wells. Fresh culture medium was thereafter added and the multi-well plates were further incubated at 37°C for 24h. This point forward, the specimens have been treated differently, in order to assess:

a) *The total biofilm (viable and dead) cells*

For the purpose of our assay, after incubation, the density of the obtained cultures recovered after the multiplication of microbial cells adhered to the tested substrata was measured at 600 nm.

b) *The viable cells embedded into the biofilms developed on different specimens*

Ten-fold dilutions were prepared from the cultures recovered after the multiplication of microbial cells adhered to the tested substrata in order to count the Colony Forming Units (CFU) and to assess the viable cell counts (VCCs) of the respective cultures. For this purpose, the adhered cells have been removed from samples by vortexing and brief sonication. Serial dilutions ranging from 10^{-1} to 10^{-30} of the obtained inocula have been spotted on Muller-Hinton agar, incubated for 24h at 37°C and assessed for VCCs. An amount of 5 µl of the chosen dilution was spotted in duplicates on the solid medium. The resulting colonies have been numbered and the average value was submitted to dilution and volume correction. The final value was expressed in CFU/mL. Performing the assay in this manner, we were able to assess the influence of different tested substrata on the adherence and the dynamics of microbial biofilm development by selected microbial strains.

CHAPTER 4. RESULTS AND DISCUSSION

4.1. Study I: Biomimetic Apatite

4.1.1. Nanopowders' characterization

From the concentration of calcium and phosphate ions, obtained by chemical analyses, we inferred the Ca/P atomic ratio in order to assess the chemical composition of synthetic BmAp after one day maturation. The obtained Ca/P atomic ratio value of 1.5, noticeably inferior to the value of 1.67, characteristic to stoichiometric HA, is similar to TCP, $Ca_3(PO_4)_2$ [4]. This puts in evidence the non-stoichiometric, calcium-deficient, biological-like nature of the apatitic (HA) phase used in our experiments.

The XRD powder patterns of pure HA (commercial powder purchased from Tecknimed SA, France) and synthetic nanocrystalline apatite maturated for one day, presented in Figure 3 exhibit the peaks specific to the analyzed samples. The XRD pattern of the BmAp powders obtained are indicative for a poorly crystallized nanoapatite, similar to mineral bone [48]. The maxima are present at the same positions as those of pure HA, but the peaks are sharper and broader.

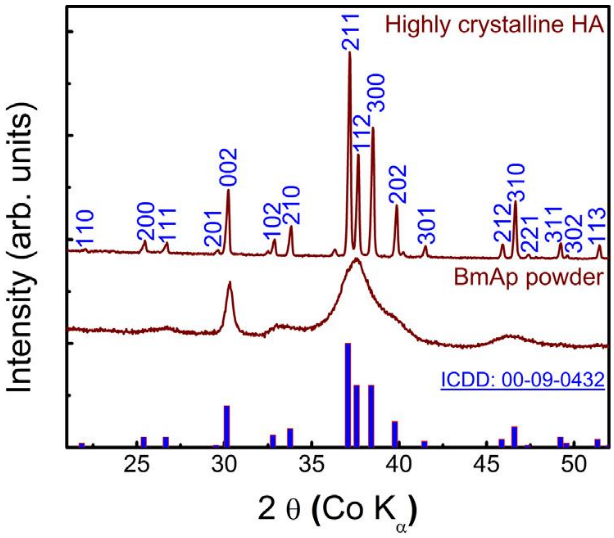

Fig. 3 XRD patterns of stoichiometric HA and BmAp one day maturated

The mean crystallite size was derived from Scherrer formula [49],

$$L_{hkl} = K^{*} \lambda / (\beta * \cos\theta) ,$$

where L_{hkl} is the mean size of the ordered (crystalline) domains, which may be smaller or equal to the grain size; K is a dimensionless shape factor, with a value close to unity; λ is the X-ray wavelength; β is the line broadening at half the maximum intensity, after subtracting the instrumental line broadening, in radians; and θ is the Bragg angle.

It was applied to diffraction lines (002) and (310), giving respectively estimated values of the crystallite length and an average of their width. Thus, if one ignores the strain effects, basic profile analysis leads to L(002) values of ~ 21 ± 2 nm, and L(310) of ~ 5 ± 2 nm, for a maturation time of one day. These data confirm the nanometer size of the crystals constitutive of synthesized apatites.

The determination of the hexagonal unit cell parameters "a" and "c" for a given specimen can provide valuable information on its closeness to the regular apatitic lattice, in respect with a reference sample, i.e. stoichiometric HA (with a = 9.41 Å and c = 6.88 Å, ICDD: 9-432). For the BmAp one day-maturated powder, the estimated crystallite size indicates a greater value of 9.45 Å for the ”a” parameter and a smaller value, of 6.85 Å, for the ”c” parameter, as compared to stoichiometric HA. We mention that the contraction of the apatite unit cell along the c-axis and expansion along perpendicular directions are generally observed in the case of nonstoichiometric, poor crystallized apatitic compounds [50].

In Figure 4 is given the FTIR spectrum of the BmAp powder. Characteristic absorption bands of nanocrystalline apatite are visible. The phosphate band positions correspond to the peaks available from literature (for stoichiometric HA) [51]. One thus notices the presence of the phosphates bands at 474 ($\upsilon_2PO_4^{3-}$), 570 and 601 ($\upsilon_4PO_4^{3-}$), 875 (υHPO_4^{2-}), 960 ($\upsilon_4PO_4^{3-}$), 1030 ($\upsilon_3PO_4^{3-}$), and 1250 cm^{-1}, respectively. The OH^- bands at 630 and 3570 cm^{-1} are also visible. Besides these, one observes the water bands at 3400-3000 and 1630 cm^{-1}. However, these peaks are less sharp and broad than the corresponding ones in the spectrum of stoichiometric HA.

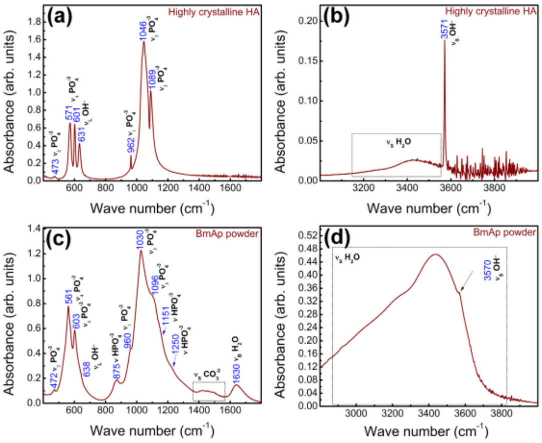

Fig. 4. FTIR spectra of BmAp maturated for one day and stoichiometric HA nanopowders

FTIR spectra of BmAp powder, after curve-fitting using Origin software, in the *v*4 PO4 domain, (Figure 5) reveal the existence of additional bands, which belong to the orthophosphate ions, which are not met in well-crystallized apatites and cannot be assigned to an apatitic environment. The formation of non-apatitic environments is associated to the synthesis of apatite nanocrystals at physiological pH in close resemblance to human body [51].

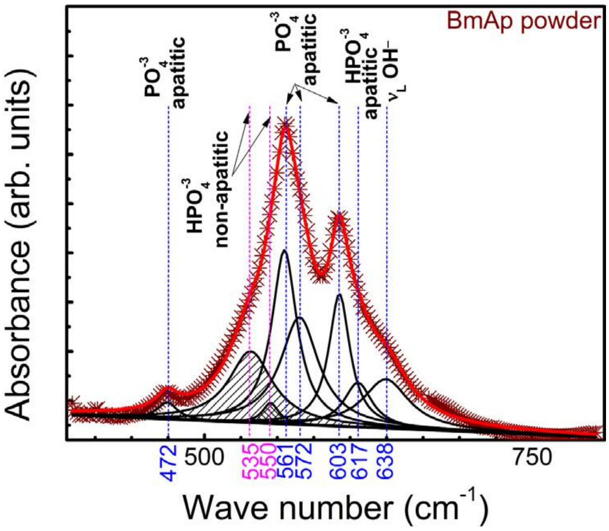

Fig. 5. Example of U_4PO_4 FTIR band decomposition (curve-fitting) using Origin software

Raman spectra were used to get additional information on the powder sample's chemical composition and structure. Two peaks were evidenced at 961 (which can be attributed to apatitic PO_4), 3675 (corresponding to apatitic OH) and a shoulder at 955 cm^{-1}, assignable to non apatitic phosphate groups. They are not observable for well crystallized stoichiometric apatites (Figure 6).

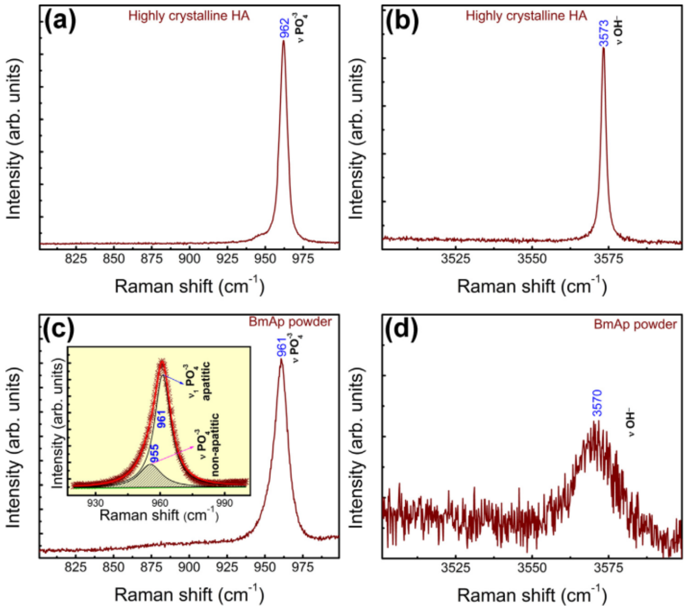

Fig. 6. Raman spectrum of BmAp thin film maturated for one day

The acicular agglomerations with 10-15 nm width and 150-250 nm length revealed by TEM (Figure 7) confirmed the nanometric nature of the constituent crystals of the powders. The powder has a homogeneous crystalline morphology.

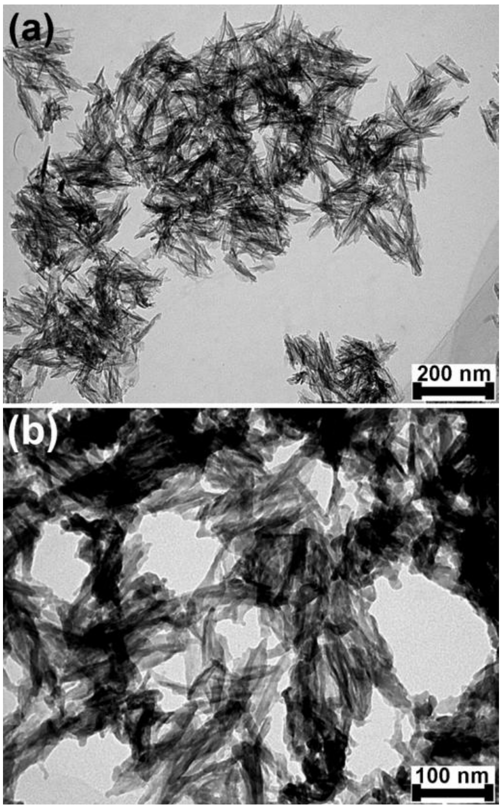

Fig. 7. TEM micrograph of HA maturated for one day

4.1..2. Characterization of deposited thin films

The deposited films were uniform at optical inspection and had an average thickness of ~ 1.2 - 1.5 μm, as evaluated after AFM inspection and 1.35 ± 0.15 μm, as measured by step profilometry [52].

Figure 8 presents the microstructure of films as visualized by AFM. The observed nanostructures contain particulates of different size from a few tens or hundreds of nm to several μm. The smaller particulates, corresponding to BmAp, were visible in large quantities, while the larger ones, fewer and better crystallized, might consist of TCP. The better crystallization and the smaller quantity could be accounted by the rather low presence of TCP. The presence of particulates, up to a few microns in size, is characteristic to structures obtained by pulsed laser technologies (PLD and MAPLE) [1, 12] and advantageous in the particular case of coated implants due to the greater interaction active surface with the surrounding cells.

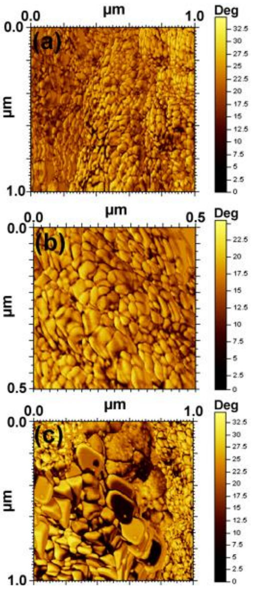

Fig. 8. Typical AFM images of deposited films recorded in tapping mode

The EDS analysis confirmed the presence of calcium and phosphorous throughout the films. The surface morphology of BmAp thin films deposited on silicon substrate was examined by SEM (Figure 9). A smooth surface was observed, consisting of particles hardly to discriminate, characteristic to films deposited by MAPLE technique [11, 12].

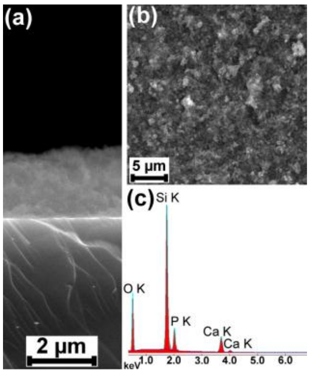

Fig.9. SEM micrographs recorded in cross-view (a) and top-view modes (b) for theBmAp MAPLE film. EDS spectrum for the BmAp MAPLE film (c).

The presence of non-apatitic environments of phosphate groups was studied by FTIR and Raman spectroscopy. The investigations put in evidence the preservation, after deposition, of the non-apatitic environments which are believed to enhance the surface reactivity, as mentioned in Ref 51.

FTIR spectra of thin films (Figure 10) were quite similar to the spectrum of the starting powder.

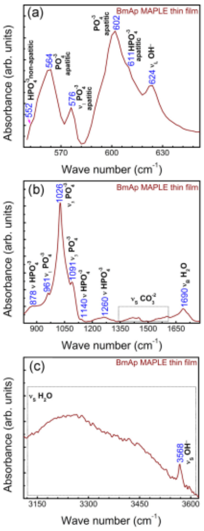

Fig. 10. FTIR spectrum of thin film of BmAp maturated for one day

We mentioned that, as in case of nanopowders, additional phosphate bands associated with the hydrated layers [51], assigned to non-apatitic chemical environments, were observed in the case of deposited films, as well.

The peaks at 474 ($\text{Ʊ}_2PO_4^{3-}$), 570 and 601 cm^{-1} (non-apatitic $\text{Ʊ}_4PO_4^{3-}$), 875 ($\text{Ʊ}HPO_4^{2-}$), 960 ($\text{Ʊ}_4PO_4^{3-}$), 1030 ($\text{Ʊ}_3PO_4^{3-}$), and 1250 cm^{-1} are assigned to characteristic FTIR absorption bands of nanocrystalline apatite.

The Raman spectra of the deposited films (Fig. not shown here) display vibrational bands characteristic to the phosphate groups. Thus, similar to powders, the same two peaks were noticed at 961 (apatitic PO_4), 3675 cm^{-1} (apatitic OH) and the shoulder at 955 cm^{-1} (assignable to non apatitic phosphate groups).

The results indicated a slight alteration only of the initial nanocrystals, the obtained films majoritary preserving the same composition as the base powder.

4.2. Study II: Ag:HA

4.2.1. FE-SEM, AFM and EDS

4.2.1.1. Morphology of Ti plates modified by TiO_2 nanotubes

As known [20], TiO_2 nanotubes fabricated by anodization method consist of patterned, strongly adherent nanostructures with an increased surface area compared to planar Ti. Such nanoscale morphology plays a pivotal role as the bone in-growth takes place preferentially in pores.

Recently, it was demonstrated for a wide variety of materials that nanostructured surfaces are enhancing the osteoblast cellular functions, improving the osteointegration response [53-55]. Superficial nanostructuring or nanoroughing can increase both the implant surface area and surface energy leading to a greater interaction of specific cell adhesion proteins [54]. Moreover, a nanoscale topography could promote unique energetic features, due to altered electron delocalizations or surface defects, acting in favor of a rapid osteointegration [56,57].

As visible from the FE-SEM micrographs (Figure 11), the anodization protocol described in anterior section lead to the uniform coating of the Ti substrate surface by a thin layer of TiO_2 nanotubes having an inner diameter of ~80 nm and outer diameter of ~100 nm.

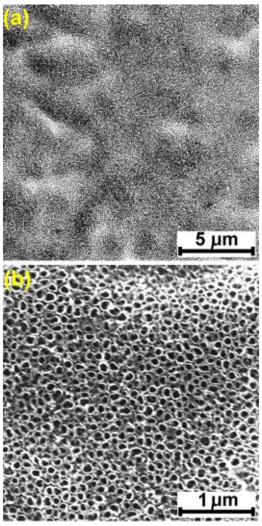

Fig. 11: FE-SEM micrographs of Ti modified by TiO_2 nanotubes obtained after anodization at 20 V for 30 min in 0.4 wt. % HF solution: general view (a) and detailed view (b).

4.2.1.2 Morphology, structure and composition of HA and Ag:HA thin films

The surface morphology, structure, composition and coating thickness of HA and Ag:HA thin films deposited on a silicon substrate were investigated by top-view FE-SEM (Fig.12), cross-view FE-SEM, AFM and EDS (Table I).

Table I: EDS elemental composition of the PLD deposited HA and Ag:HA thin films.

Element	Intensity	Concentration [at. %]	Intensity	Concentration [at. %]
	HA		Ag:HA	
C K	0.0102	10.3	0.0151	9.18
O K	0.0501	52.13	0.1128	51.98
SiK	-	-	0.0009	0.09
P K	0.1587	14.53	0.1889	15.63
Ca K	0.3708	23.31	0.3474	21.71
Ag L	-	-	0.0077	0.22

Ca/P	-	1.60	-	1.39

Well-distinguishable spherical particulates (150 – 1500) nm in size were observed for both HA and Ag:HA films (Fig. 12). The more flattened particles resulted due to the energetic impact with the substrate.

According to current PLD physics models [30,58], such particulates are either expulsed directly from target by phase explosion, plasma recoil and surface instabilities or are forming by coalescence of particles due to intense collisions during the transit from target to substrate. A significantly higher density of particulates was observed for the Ag:HA films (Figure 12b).

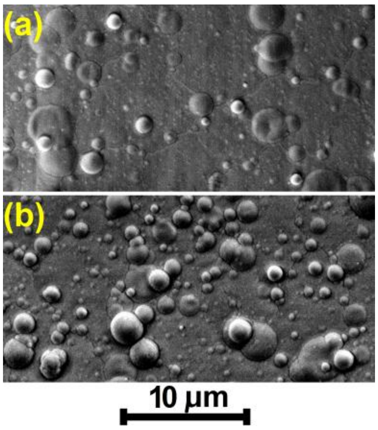

Fig. 12: Top-view FE-SEM micrographs of the HA (a) and Ag:HA (b) coatings deposited by PLD on Si <111> mirror polished wafers.

At the same laser fluence, if assuming a lower melting point for the Ag:HA (less crystalline than the pure HA, as will be shown further), the increased number of particulates found on the Ag:HA film surface can be the result of the phase explosion process (explosive boiling) due to the surface superheating, at temperature approaching the thermodynamic critical point.

The abundant presence of these particulates leads to the strong increase of surface roughness, and can result in a superior *in situ* anchorage of the implant, thus preventing micro-movements of the medical device and providing the necessary initial stability until bone will grow and attach to the implant surface.

Based upon the cross-section micrographs, the thickness of the two films was estimated at ~1.44±0.1 μm (for HA) and ~1.64±0.1 μm (for Ag:HA), respectively.

From a qualitative point of view, the EDS spectra of the HA based films (data not shown) indicated the presence of typical apatite elements, only (Ca, P, O, C), along with the signal originating from the Si substrate. In the case of Ag:HA coating, except the characteristic HA elements, Ag presence was also emphasized. The absence of other cations asserts the films purity.

The EDS quantitative data were collected in Table I. A slight decrease of Ca/P atomic ratio in the pure HA films with respect to the theoretical HA stoichiometry (Ca/P=1.67), can be noticed. However, because the renown limited accuracy of the EDS analysis technique, one should treat such quantitative results with caution. The decrease of the Ca/P atomic ratio from 1.60 in HA film to 1.39 in Ag:HA film, pleads in favour of the substitution of a part of Ca ions by silver ions. We note that the Ca/P atomic ratio for the HA pure or doped films synthesized by PLD is dependent on substrate temperature and incident laser fluence [59].

Next, the surface morphology of Ag:HA films was investigated in higher detail by AFM. High resolution AFM images (not shown here) evidenced that the films consisted in fact of quite small and tightely packed spheroidal grains. The thin Ag:HA films exhibited quite similar morphologies irrespective of the type of substrate used. The absolute roughness (R_a) was of ~28 nm for Ag:HA/Ti and of ~29 nm for Ag:HA/nTiO_2/Ti structures. It is therefore resulting that the substrate morphology has a reduced influence on coating roughness. This is to be expected in case of thick films (in our case of ~1.5 µm). When increasing the thickness, the growing film tendency to mimic the substrate relief is reduced, so that if the thickness becomes large enough, the film morphology is mainly determined by the physical/chemical deposition processes. At nanometric level, the roughness is mainly determined by the contribution of the smaller droplets, from which the entire film envelope (matrix, and embedded larger droplets) is composed. We mention that before deposition, the roughness of Ti and Ti modified with TiO_2 nanotubes substrates was of 7 and 20 nm, respectively. According to Narayanan *et al.* [60], a low scale HA coating roughness can decrease the contact angles and can aid in good attachment of osteoblasts to metallic substrates. It follows that the deposited Ag:HA thin films exhibit a convenient nanostructuring for bone implants.

4.2.2. FTIR

Figure 13 displays the FTIR spectra recorded in case of HA (a,c) and Ag:HA (b,d) films deposited on Ti (a,b) and Ti modified by TiO_2 nanotubes (c,d), before and after the post-deposition heat treatment.

All IR spectra are dominated by the vibration effects of the various Q^n phosphate species, which cover the entire (1400–400) cm^{-1} wave numbers region [61]. The threefold degenerate ν_3 stretching of phosphate stands for the typical prominent vibration band of HA and consists of at least three sub-modes [62].

In the case of HA/Ti and Ag:HA/Ti as-deposited samples (Figure 13ab), the band centered at (938–937) cm^{-1} corresponds to the ν_1 non-degenerated symmetric stretching of phosphate groups, while the bands positioned at (964–963), (1029–1021), (1088–1087) cm^{-1} belong to the degenerated ν_3 asymmetric stretching vibrations of phosphate groups [61,63]. The peaks at (561–558) and (599–598) cm^{-1} are due to the degenerated ν_4 asymmetric bending vibration of phosphate group. The ν_3 and ν_4 $(PO_4)^{3-}$ vibration bands are considered the IR fingerprint of a HA structure. In the case of HA/nTiO_2/Ti and Ag:HA/nTiO_2/Ti samples, similar FTIR envelopes were recorded (Fig. 13cd), displaying the same vibration bands. To the difference of films deposited on TiO_2 nanotubes arrays, for the films deposited on pure Ti it was possible to emphasize the symmetric stretching vibrations of PØP groups in Q^3, Q^2 and Q^1 units, as a faint band centered at ~800 cm^{-1} . The low intensity band positioned in the range of (875–870) cm^{-1}, for all as-deposited films, is the indicative of HPO_4^{2-} impurity ions presence. The broad and low intensity band situated in the range of (1600–1300) cm^{-1} can be attributed to the ν_3 antisymmetric stretching vibrations of carbonate functional groups. This can be caused by the possible sample contamination during handling. The undefined noisy aspect of this region suggests the presence of carbonate groups on both sites [A-type substitution refers to the $(CO_3)^{2-}$ in the OH^- sites, whilst the B-type substitution is due to $(CO_3)^{2-}$ replacing $(PO_4)^{3-}$ ions without an adjacent OH^- ion [62]. The ν_4 and ν_1 vibration modes of carbonate can be rarely detected because of their very weak intensities, whilst ν_2 bending band, generally situated at ~875 cm^{-1}, with an intensity about one fifth that of ν_3 band, is obscured in our case by the acid phosphate band [63]. Moreover, one can infer that the as-deposited films are strongly dehydrated, as neither structural (deformation ν_L or stretching ν_S) nor absorbed water (bending and stretching) vibration modes have been observed on the entire (4000–550) cm^{-1} range. It is known that the atomic disorder in the apatite lattice impedes the incorporation of OH^- ions [64].

The regular shifts of the bands in the case of Ag:HA films suggest the occurrence of a series of short-range order structural modifications. The broadening of vibration bands, emphasized for the all the as-deposited films, can be associated with a low local symmetry and high atomic disorder.

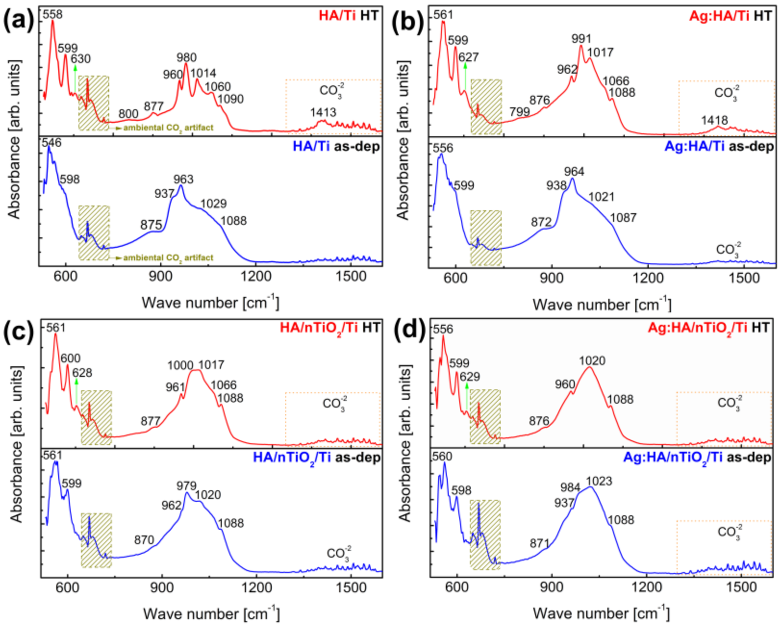

Fig. 13: FTIR spectra of HA (a) and Ag:HA (b) films deposited on Ti substrates, HA (c) and Ag:HA (d) films deposited on Ti modified by TiO_2 *nanotubes substrates, before and after the thermal treatment.*

After the post-deposition heat-treatment, one notices a remarkable modification of spectra profile. The vibration bands became sharper, and the peaks are better resolved. The splitting of the ν_4 bending and ν_3 stretching modes of phosphate denote an improvement of the crystalline status of the HA films. This phenomenon manifests more radically in case of films deposited on bare Ti substrate. The shifting of the absorption bands after annealing could be explained by a modification of the crystalline/amorphous phase ratio. The phosphate bands shifted closer to the positions characteristic to a HA standard structure, thus pointing to an improvement of the tetrahedral structure of the phosphate ions. The new band peaking at ~630 cm^{-1}, originating from the libration mode of hydroxyl group, highlighted the presence of structurally bound OH^- in the apatitic films. This is a supplementary proof of the efficiency of the post-deposition heat-treatment in promoting the reconstitution of HA in terms of composition and structure. Because the HPO_4^{2-} ions are known to be lost in the 160–240 °C temperature range [65], the low intensity sharp peak arising at ~(877–876) cm^{-1}, for the heat-treated films, can be solely associated to the ν_2 bending vibration of carbonate. This assumption is backed by the correlated rise and evolution of the bands due to ν_3 stretching vibration of $(CO_3)^{2-}$ groups (~1415 cm^{-1}) (Fig. 13ab *vs*. Fig. 13cd). The positions of the carbonate bands indicate the predominance B-type substitution in the crystal lattice of HA [63]. The B-type is the preferential substitution in the human bone and is known to have better bioactivity and osteoinductivity [66]. The carbonatation could arise from the signaled contamination of the as-deposited samples, but more likely is potentiated by the easiness of substitution of $(PO_4)^{3-}$ by $(CO_3)^{2-}$ ions during the post-deposition thermal processing.

4.2.3. XRD

The XRD analyses evidenced the hexagonal HA (space group $P6_3/m$; ICDD file: 00-009-0432) as the predominant crystalline phase in all films (Fig. 14). The most intensive peaks of the patterns were the Ti peaks of the substrate (ICDD file: 00-044-1294). The intensity scales of the graphical representations were therefore chosen to emphasize the lower intensity lines originating from the deposited films.

In case of as-deposited films, the broad and shallow HA peaks, are indicative of the poor crystallization under the used deposition condition. All the as-deposited PLD films contained a significant amorphous component, as revealed by the pronounced halo centered at $2\theta\approx31°$. Exceptionally, the XRD patterns of the HA/Ti and Ag:HA/Ti as-deposited films revealed the presence of a supplementary peak, positioned at $2\theta\approx36.2°$, which can be best associated to a titanium sub-oxide phase (TiO, ICDD file: 01-086-2352), as superficial product of the Ti substrate fabrication. Indeed, the bare Ti substrate diffractogram (black line – bottom of Fig. 14a), showed besides this 111 reflection, other TiO reflection as well, 200 at $2\theta\approx42.06°$, accessible in the scanned angular range. This latter TiO reflection, is more difficult to discern in the case of HA coated Ti substrates, because of the superposition with the 311 peak of HA ($2\theta\approx42.03°$). After the post-deposition heat-treatment, this peak disappeared in the case of HA/Ti samples, or has a lower intensity in the case of Ag:HA/Ti samples.

In the case of films deposited on nanotubes arrays, no crystalline TiO_2 phases could be detected, supporting the amorphous status of these as-anodized nanostructures, in good accordance with literature [67].

After the post-deposition heat-treatment, the XRD patterns revealed a remarkable increase of films' crystallinity (Figure 14). The PLD films were converted to a monophasic HA structure with various crystalline features, depending on the type of substrate and on the HA nature (pure or silver doped). As known, the enhanced crystallization inhibits HA dissolution in body environment and contributes to an improved osseous tissue growth [68]. The absence of impurity phases confirmed that decomposition of HA and Ag:HA thin films did not occur as an effect of the thermal treatment.

In case of the Ag:HA/nTiO_2/Ti heat-treated samples (Fig. 14d) only, one can note the presence of the most important diffraction lines of two of the TiO_2 polymorphs: 101 anatase and 110 rutile. The absence of such phases in the case of HA/Ti and HA/nTiO_2/Ti heat-treated samples (Fig. 14ac), together with the aforementioned evolution of titanium sub-oxide phase, suggest that the Ag:HA layers might be more pervious for ambient oxygen in-diffusion during heat-treatment. The pure HA layers are denser, efficiently sealing the substrate, and thus avoiding the substrate direct contact with free oxygen during the heat-treatment process.

One can speculate that during heating, the less stable TiO phase present at the Ti-apatitic film interface (Figure 14ab) could dissociate, and the Ti and oxygen atoms could break from their precarious structural arrangement. The oxygen atoms can be easily consumed during the structural and compositional restoration of HA films. When the films are less compact (supposedly the case of Ag:HA films), this kinetic trend can be counterbalanced by free oxygen penetration from the ambient, reflected in persistence of TiO phase in the case of Ag:HA/Ti samples (Figure 14b), or the crystallization and possible growth towards the more oxygenated surface of the TiO_2 nanotubes (Figure 14d). In the case of an impervious layer (the case of pure HA films – Figures 14ac), the oxygen diffusion through films from the ambient is hindered and the driving force of TiO_2 formation and crystallization is significantly reduced.

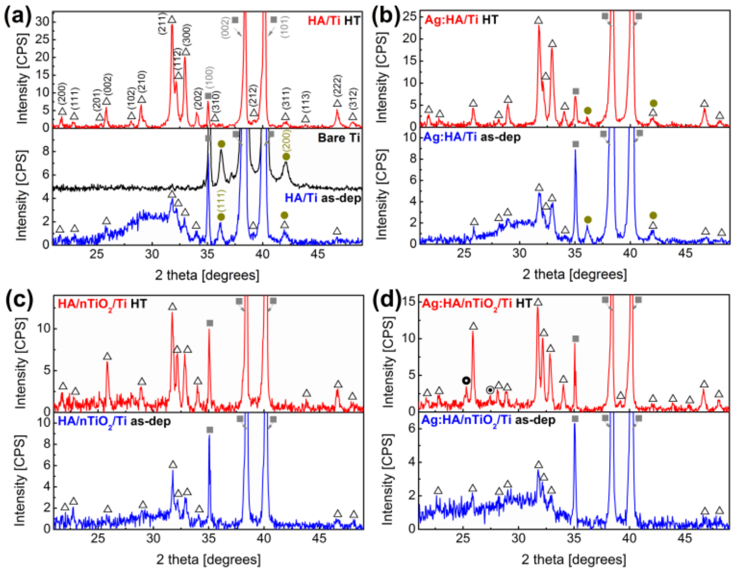

Fig. 14: XRD patterns of HA (a) and Ag:HA (b) films deposited on Ti substrates, HA (c) and Ag:HA (d) films deposited on Ti modified by TiO_2 nanotubes substrates, before and after the thermal treatment. (□=Ti – ICDD: 00-044-1294; □= $Ca_{10}(PO_4)_6(OH)_2$ (hydroxyapatite) – ICDD: 00-009-0432; □=TiO (titanium sub-oxide) – ICDD: 01-086-2352; ⭘=TiO_2 (anatase) – ICDD: 00-021-1272; ⊙=TiO_2 (rutile) – ICDD: 00-021-1276).

No remarkable line shifts (thus no noteworthy modification of the interatomic distances in the lattice) were noticed for Ag:HA film as compared to HA films. This was to be expected for such low levels of doping, as the diameter of the substituting silver ions is only slightly larger than the diameter of the calcium ion (Ag^{2+}/Ca^{2+} ionic radii ratio=1.09).

In good agreement with the FTIR results, the XRD measurements revealed that the post-deposition heat-treatment contributed to the amelioration of the crystalline status of both HA and Ag:HA thin films regardless of substrate nature. However, in case of films deposited on bare Ti, the Ag doping seems to slow the crystallization rate (Fig. 14ab and Table II). This result is in accordance with the results of Ciobanu *et al.* study [69]. The reduced X-ray scattered intensity in case of HA and Ag:HA films deposited on anodized Ti substrates, supported their lower crystallinity, and advocated for a substrate nature – film crystallinity dependence.

The mean crystallite size, approximated on the basis of the FWHM of the (002) and (300) crystal planes reflections by applying the Scherrer formula [70] (Table II), fully supports these hypotheses. The lines' width was corrected for instrumental broadening using a CeO_2 laboratory reference. The peaks' broadening due to the film inner strain was not considered. The crystallite size determined from the 002 line breadth stands for the dimension parallel to the *c-axis*, while the crystallite size determined from the 300 line breadth corresponds to the dimension projected in the basal plane.

Table II: Mean crystallite sizes estimated from the FWHM of the (002) and (300) crystal planes reflections, by applying the Scherrer formula.

Sample type	Space group	D_{002} [nm]	D_{300} [nm]	D_{002} / D_{300}
HA PLD target	Hexagonal, $P6_3/m$ (176)	51.8	17.2	~3.01
Ag:HA PLD target		32.5	10.6	~3.07
HA/Ti heat-treated		74.2	50.3	~1.47
Ag:HA/Ti heat-treated		62.3	35.8	~1.74
HA/nTiO_2/Ti heat-treated		42.6	37.0	~1.15
Ag:HA/nTiO_2/Ti heat-treated		54.1	49.3	~1.10

The crystallites growth was anisotropic in shape, being apparently influenced by the substrate nature, their average size decreasing in the presence of the TiO_2 nanotubes arrays. Rather similar D_{002} / D_{300} ratios were obtained when using the same type of substrate, irrespective of film type (pure or doped). The anisotropy of the apatitic films decreases when deposited on TiO_2 nanotubes (Table II).

As compared to the parent targets, the shape factor (D_{002} / D_{300}) is reduced (the crystallites becoming more oblate): two times in case of films deposited on bare Ti, and three times in case of films deposited on Ti modified by TiO_2 nanotubes (Table II).

On the basis of these results, one may expect a substantial improvement of bioactive behavior in case of Ag:HA/nTiO_2/Ti heat-treated sample as stimulated by their structural development. These depositions were therefore selected for biological assays.

4.2.4. Biological assays

Our studies of cytotoxicity showed that the tested biomaterials do not influence the cellular adhesion, viability, morphology and proliferation rate. Their development onto the tested material surfaces is similar to the glass control (Figure 15).

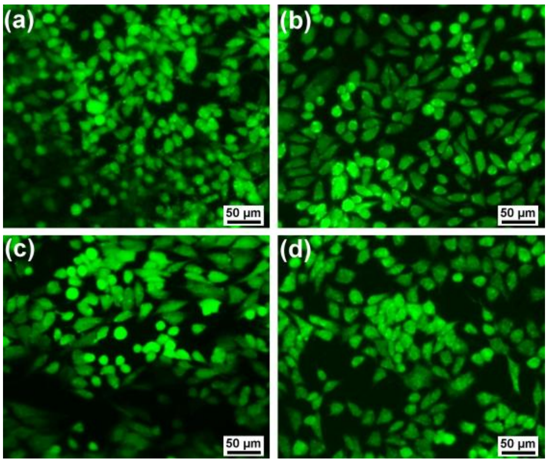

Fig. 15: Fluorescence microscopy images of HEp2 cells grown on different samples: glass control (a); Ti substrate (b); nTiO_2/Ti substrate (c); and Ag:HA/nTiO_2/Ti structure (d).

Through the DNA quantification by flow cytometry the cells are divided in three categories: G1 (normal cells), S (cells that have started DNA synthesis in order to divide) and G2 (cells that have terminated DNA replication and will undergo mitosis). The proliferation index (I_p) is currently defined as the percent of cells that have started and finished the DNA replication [I_p=(S+G2)*100/(G1+S+G2)]. As seen in Table III, there are no relevant differences regarding proliferation between the tested biomaterials and glass control.

Table III: Cellular cycle phases of HEp2 cells grown on investigated biomaterials and glass control.

Sample	G1 (%)	S (%)	G2 (%)	I_p (%)
Glass control	70.7	20.18	9.12	29.30
Ti	72.09	19.00	8.91	27.91
nTiO_2/Ti	70.87	20.22	8.91	29.13
Ag:HA/nTiO_2/Ti	70.21	20.51	9.28	29.79

Following the results of physical-chemical investigations and cytotoxicity tests, we selected for antifungal testing the heat-treated Ag:HA thin films deposited on modified by TiO_2 nanotubes substrates. The obtained results in case of *Candida albicans* and *Aspergillus niger* strains are given in Figure 16 and summarized in Table IV against control.

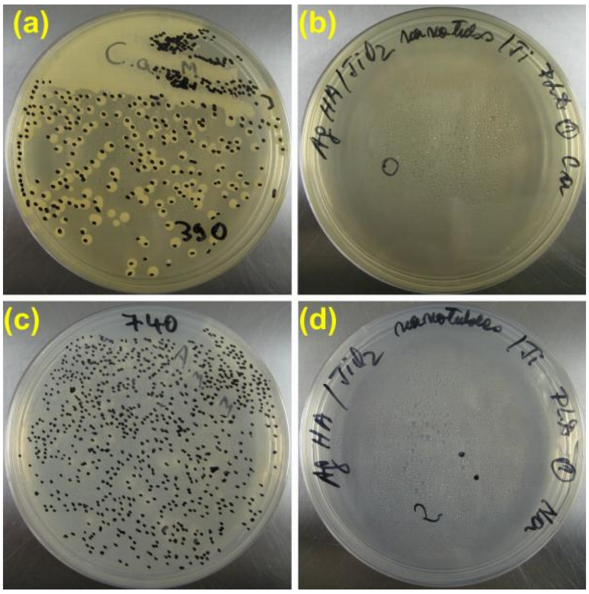

Fig. 16: Comparative photographs of fungal populations (Candida albicans – a,b; Aspergillus niger – c,d), 24 hours after incubation, on the heat-treated Ag:HA/nTiO_2/Ti films (b,d) and standard control samples (a,c).

Table IV: Percentage of reduction rate for Candida albicans and Aspergillus niger colonies incubated on the Ag:HA/nTiO_2/Ti heat-treated films compared to control.

Sample	*Candida albicans* [% reduction]	*Aspergillus niger* [% reduction]
Control	0	0
Ag:HA/nTiO_2/Ti	100	99.73

From the results presented in Figure 15 and Table IV it follows that the heat-treated Ag:HA thin films deposited on Ti modified by TiO_2 nanotubes substrates have a radical antifungal action against the two strains, causing the reduction of colonies by 99.73% in case of *Aspergillus niger* and a complete extermination in case of *Candida albicans* colonies. At the same time, the fungi colonies incubated on control surfaces where unperturbed and survived integrally.

Identical microbiological tests carried out with Ag:HA coatings directly deposited on

Ti substrates (results not shown) evidenced a lower antifungal activity (by several tens of percents). These results are in good agreement with data published by Li *et al.* [71] for dental implantologic materials (Ti and pure HA among others).

4.3. Study III: Ag-Lig:HA

4.3.1 SEM-EDS

Typical top-view SEM images of the HA-Lig and Ag-Lig:HA films are displayed in Figure 17. MAPLE deposition resulted in rather smooth films with a homogenous and pore-free microstructure, without particular morphological features. Rough surface of the films was reported starting from the same nanohydroxyapatite powder composite with Lig, when using the electrophoretic deposition [72]. As an important note, no remarkable morphological differences have been evidenced between the HA-Lig and Ag-Lig:HA films.

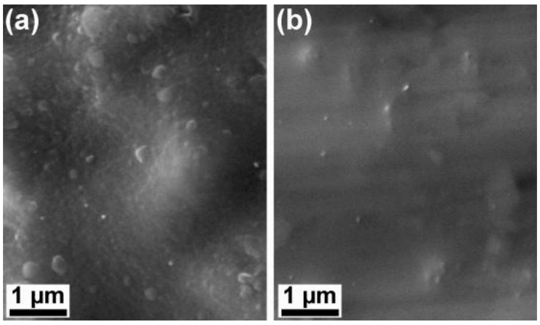

Fig. 17.Top-view SEM micrographs of the HA-Lig (a) and Ag-Lig:HA (b) films deposited onto TiO_2/Ti substrata by MAPLE. Inset: cross-view SEM micrograph of Ag-Lig:HA film deposited onto silicon wafer.

The cross-sectional SEM images collected in case of films deposited onto Si wafers, revealed the compact look of these MAPLE coatings with good adhesion to the substratum. A thickness of ~180±10 nm has been estimated based upon the cross-sectional SEM analyses. A typical cross-SEM image of the Ag:HA-Lig film grown on a silicon wafer is visible in Figure 17b-inset.

The qualitative EDS analyses (data not shown) revealed the high purity of films and indicated the presence of all elements of HA, along with carbon content for both types of films, suggesting the incorporation of Lig. Small traces of Ag have been detected in the case of Ag:HA-Lig films. The quantitative EDS estimation indicated the synthesis of a calcium deficient HA phase, as the atomic Ca/P ratio was slightly altered during the ablation process down to a value of ~1.33 (inferior to 1.67 theoretical Ca/P ratio, characteristic to stoichiometric HA). Such a deviation could be associated with Ca/P ratio dependence on substratum temperature and laser incident fluence [73,74,75]. Small traces of Ag (~0.57 wt. %) have been detected in the case of Ag:HA-Lig films. However, because of the low accuracy of the EDS technique, this value should be considered as a rough approximation only.

4.3.2 XRD

The GIXRD patterns revealed the Ti substratum maxima only, suggesting that the TiO_2 nanotubes, as well as the HA-Lig and the Ag:HA-Lig coatings synthesized by MAPLE were amorphous within the experimental sensitivity limit of the apparatus. A typical GIXRD pattern (for the Ag:HA/TiO_2/Ti film) is presented in Fig. 18. For comparison, the reference files of hydroxyapatite (ICDD: 00-009-0432), anatase (ICDD: 00-021-1272) and rutile ((ICDD: 00-021-1276) are superimposed on the graph.

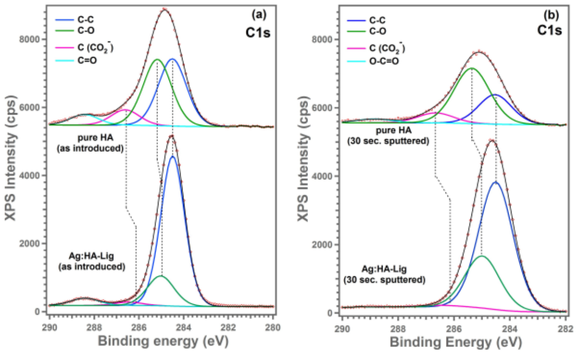

Fig. 18: Typical GIXRD pattern of a Ag-Lig:HA /TiO_2/Ti film deposited by MAPLE.

4.3.3 XPS

The XPS spectra were recorded for the pure HA, HA-Lig and Ag:HA-Lig films. As known, charging effects may arise during measurements, resulting in an apparent shift of core-level XPS lines [76]. Mitigating this effect usually involves using a flood-gun corroborated to overall shift of all lines with values that correlate to C1s line at 284.5 eV, considered as standard. In our case such calibration is difficult since C1s band has a complex structure, featured by several components. In fact, their assignment is essential in identifying the Lig signature in the XPS spectrum.

In order to identify the contamination-associated component, a 30 s Ar^+ sputtering was performed at accelerating voltage of 3 kV resulting in an ion current of ~$15x10^{-6}$ A. Assuming that every incoming ion pulls-out a surface atom, one estimates that in 30 s we remove 2 nm approximately from the surface layer. Based on this assumption, we expect that the signature provided by C1s spectrum entirely belongs to pure HA, HA-Lig and Ag:HA-Lig composite films, free of any contamination. Consequently, C-bonded carbon line was identified as the component with the most evident intensity drop-off, and it was kept at 284.5 eV and used as calibration line.

The presence of Lig was demonstrated in both HA-Lig and in the more complicated case of Ag:HA-Lig. For discussion, we therefore focused on a comparison of the XPS data between pure HA and Ag:HA-Lig coatings. The intensity variation of the C1s XPS components after the sputtering cycle is given for the two cases (Figure 19). The Lig signature was revealed to be dispersed in the HA matrix, as evidenced by a massive increase of the C-bonded carbon signature, accompanied by a slight increase of the component associated with oxygen-bonded C or oxygen-containing radicals (Table V).

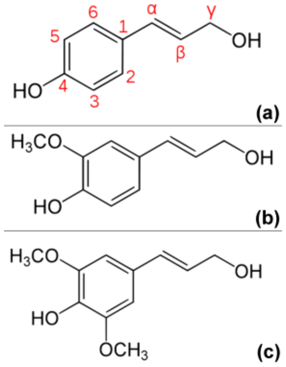

Fig.19: Theoretical stoichiometry and chemical formulas of the three monolignols: (a) hydroxyphenyl ($C_9H_{10}O_2$), (b) guaiacyl ($C_{10}H_{12}O_3$) and (c) syringyl ($C_{11}H_{14}O_4$) [36].

Table V: C 1s XPS core level sub-components areas.

	%C for “as-introduced” samples				%C for 30 s. sputtered samples			
Pure HA	C-C/ C-H	C-OH/ C-OR	C=O/ HO-C-OR	C=O	C-C/ C-H	C-OH/ C-OR	C=O/ HO-C-OR	C=O
	41.86	41.79	9.70	6.65	28.33	57.37	10.35	3.95
Ag:HA-Lig	76.7	17.08	1.91	4.31	70.42	27.10	2.48	-

The indisputable proof that the Lig has been effectively transferred into the HA composite film would consist in determining the experimental stoichiometry fraction xC:yO from the XPS data considering the addition of 10% Lig into the HA matrix.

From the experimental stoichiometry inferred for the pure HA case aC:bO and that of the HA-Lig composite 0.9[aC:bO]+0.1[xC:yO], the values obtained were x=11, y=4.4. These values closely correspond to the Lig theoretic stoichiometry of the three monolignols ($C_9H_{10}O_2$/$C_{10}H_{12}O_3$/$C_{11}H_{14}O_4$) (Figure 19) which lead to Lig formation by polymerization. As a crosscheck and as suggested in previous studies [77-79], we have also calculated the theoretical stoichiometry of the dopant using the integral amplitudes of the C1s and O1s peaks. Comparable results have been obtained, i.e. x=11, y=3.75. These findings validate the experimental results.

4.3.4 ATR-FTIR

FTIR spectroscopy was applied for identifying the functional groups and the degree of short-range ordering in the deposited films. Emphasis was put on identifying the distinct chemical bonds of Lig and the degree of macromolecule decomposition during MAPLE transfer, if any.

The ATR-FTIR spectra of the original Lig powder, pure HA powder, and pure HA and Ag:HA-Lig films (deposited under optimized conditions) are shown comparatively in Fig. 20. The assignment for the IR vibration bands is given in Table VI.

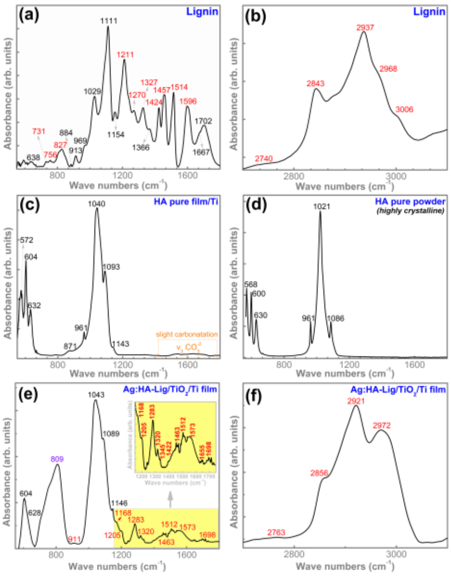

Fig. 20: ATR-FTIR spectra of Lig powder (a,b), pure HA film (c), pure HA powder (Sigma-Aldrich) (d) and Ag:HA-Lig film (e,f) in the spectral regions: 1800 – 550 cm^{-1} (a,c,d,e) and 3100 – 2700 cm^{-1} (b,f).

Table VI: Assignment of ATR-FTIR vibration bands for the lignin powder, pure synthetic HA powder (Sigma-Aldrich), pure HA film, and Ag:HA-Lig composite film.

Observed IR bands (cm^{-1})				Bands' assignment
Pure Lig	*Pure HA powder*	*Pure HA film*	*Ag:HA-Lig film*	
–	568	572	604	asymmetric bending (ν_4) of $(PO_4)^{3-}$ groups
–	600	604		asymmetric bending (ν_4) of $(PO_4)^{3-}$ groups
–	630	632	628	librational mode of $(OH)^-$ groups
638	–	–	–	C-OH out-of-plane bending
731	–	–	–	C-H bonds on the benzene rings
756	–	–	749	asymmetric bending of HCCH groups
–	–	–	809	Ti–O vibrations
827	–	–	–	C-H out-of-plane in position 2 and 6 of syringyl (S) and in all positions guaiacyl (G) units
–	–	871	–	vibrations of $(HPO_4)^{2-}$ ions
884	–	–	–	C-H deformation vibration of cellulose
913	–	–	911	C-H bending of S units
–	961	961	942	symmetric stretching (ν_1) of $(PO_4)^{3-}$ groups
969	–	–	–	=CH out-of-plane deformation
1029	–	–	–	C-O stretching of cellulose
–	1021	1040	1043	asymmetric stretching (ν_3) of $(PO_4)^{3-}$ groups
–	1086	1093	1089	asymmetric stretching (ν_3) of $(PO_4)^{3-}$ groups

1111	–	–	–	C=O stretching
–	–	1143	1146	vibrations of $(HPO_4)^{2-}$ ions
1154	–	–	1168	C-O-C asymetric stretching in cellulose
1211	–	–	1205	C-C, C-O and C=O stretching of G units
1270	–	–	1283	C-O stretching of G units
1327	–	–	1320	C-O stretching of S units
1366	–	–	1345	C-H symmetric bending in cellulose
1424	–	–	1422	C-H in plane bending in Lig
1457	–	–	1463	C-H bending of methyl and methylene groups
1514	–	–	1512	C=C stretching of the aromatic ring (G)
1596	–	–	1573	C=C stretching of the aromatic ring (S)
1667	–	–	1655	C=O stretching in conjugated p-subst. aryl ketones
1702	–	–	1698	C=O stretching in unconjugated aldehyde, ketone, carbonyls or ester groups
2740	–	–	2763	aldehyde C-H stretch
2843	–	–	2856	asymmetric CH stretching in aromatic methoxyl groups and in methyl and methylene groups of side chains
2937	–	–	2921	symmetric CH stretching in aromatic methoxyl groups and in methyl and methylene groups of side chains
2968	–	–	2972	sp^3 hybridized C-H
3006	–	–	–	sp^2 hybridized C-H

In the fingerprint region (1800–550 cm^{-1}), Lig powder exhibits an intricate spectrum with numerous sharp and discrete absorption bands due to its main molecular components (Table VI). HA-Lig and Ag:HA-Lig coatings had similar envelopes dominated by the typical vibration bands of HA [80]: the ν_4 symmetric bending, ν_1 symmetric and ν_3 asymmetric stretching modes of phosphate groups, along with the libration mode of structural OH (see Table VI). Because of the complex composition of Ag:HA-Lig coatings, we chose to present in Fig. 5e the IR spectrum of this film only.

In the (1200–550) cm^{-1} wave number region the prominent HA bands are superimposed to some of the Lig bands, partly obscuring them. Moreover, in the (890–660) cm^{-1} region, the intense band of the Ti-O and Ti-O-Ti skeletal vibrations is brought in by the underlayer of TiO_2 nanotubes [81]. However, the Lig contribution can be hinted by a more complex shape of the IR envelope in the case of Ag:HA-Lig composite film (Fig. 20e) with respect to the pure HA film and powder spectra (Fig. 21c,d).

The undeniable evidence of the Lig macromolecule transfer is revealed by the distinct bands of Lig visible in the (1800–1200) cm^{-1} (Fig. 20a,e&e-inset) and the (3100–1200) cm^{-1} (Fig. 20b,f) wave number regions [82-84]. The presence, in these specific spectral regions, of all Lig vibration bands, suggests that the Lig material is not altered during the MAPLE transfer, the slight shifts being induced rather by the molecular interactions with the HA matrix than by its degradation.

The broader IR spectrum in the case of Ag:HA-Lig composite film also indicates that a short-range ordering alteration occurred as a consequence of intermolecular interactions between the HA film matrix and the Lig components. Differences in the absorbance values and shape of the bands were also detected in the infrared spectra, pleading as well for intimate structural modification induced by the Lig embedment in the HA film matrix.

The stretching modes of guaiacyl (G) and syringyl (S), archetypal for Lig, were evidenced in the composite films at the 1205 (G), 1283 (G), and 1320 cm^{-1} (S) respectively. The guaiacyl IR bands are dominant which suggests that a larger amount of G units is present in the film. Higher G/S ratios could increase cross-linking of the Lig molecules [83] dispersed in the entire HA matrix, and thus, could contribute to the augmentation of the mechanical properties of the film and a more durable composite material.

4.3.5 Effect of the prepared samples on WJ-MSCs viability

Stem cells and progenitor cells are promising candidates for the development of efficient therapeutic and regenerative strategies, with a large spectrum of clinical applications, including biomaterials and tissue engineering [84]. MSCs are adult stem cells able to differentiate into a variety of cell types *in vitro*, but also to engraft *in vivo* [85,86]. We therefore decided to use MSC for our *in vitro* cytotoxicity tests, with the conviction that the results would be a solid foundation for future *in vivo* biocompatibility studies of the MAPLE coatings.

We would like to emphasize that no significant changes were observed in the morphology of WJ-MSCs, when grown on the surface of the tested materials. The experiments have shown that the MAPLE composite coatings exhibited no toxicity towards human cells and allowed a sustained growth of WJ-MSCs.

It appears that the presence of Lig improves the biocompatibility of the HA coated TiO_2/Ti, by promoting the growth of adhered cells, clearly supporting the suitability of our composites for developing future biomaterials with increased biocompatibility (Figure 21).

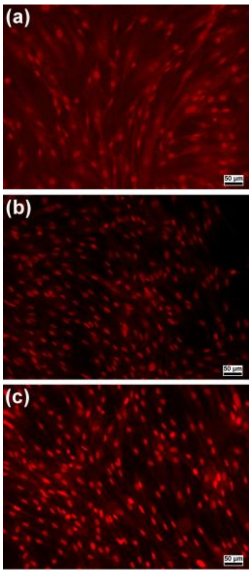

Fig. 21: Fluorescence microscopy images of nuclei of WJ-MSCs grown on different substrata: pure HA (a); HA-Lig (b); and Ag:HA-Lig (c) films. Magnification: 200X

4.3.6 Microbial assay results

Our initial hypothesis was that adding Lig to HA-films doped with Ag ions would yield a material with improved antimicrobial properties. To test this hypothesis, we have examined the anti-biofilm efficiency of the bioactive composite coatings, by using two well-established microbiological assays. One is based upon the assessment of VCCs, whilst the second resorts to bacterial culture density measurements, for the quantification of total microbial biofilm developed on the materials obtained at different time intervals, i.e. 24h, 48h and 72h respectively. These two approaches could provide complementary information regarding the number of viable cells embedded in the biofilm (viable cell counts) as well as the density of microbial biofilm (comprised of both viable or dead cells).

The temporal dynamics of biofilms formed by microbial species, either fungi or bacteria are different, as it is their resistance to various antimicrobial agents [87,88]. However, research performed in many biofilm-forming organisms has revealed that the development of a biofilm is a two-step process involving an initial attachment and a subsequent maturation phase, which are physiologically different from each other and require phase-specific factors. A final dispersal phase involves the detachment of single cells or cell clusters promoting the bacterial dissemination [89]. In the maturation phase, bacterial cells proliferate and produce an extracellular matrix consisting of several secreted polymers, such as exopolysaccharides, teichoic acids and specific proteins, as well as DNA originating from the lysed bacteria [90].

The observed dynamics of *S. aureus* biofilm formation varied depending on the tested specimen.

The biofilm developed on the pure HA coating control specimen showed a growth peak at 48h, the number of viable bacterial cells recovered at 48h remaining practically constant at 72h (Figure 22a).

At 24h, the number of viable cells harvested from the HA-Lig and Ag:HA-Lig samples slightly increased with respect to control, by 3 to 4 logs (Figure 22a). At 48h, the number of viable cells embedded in the biofilm developed on the HA-Lig still showed increased values exceeding by 4.5 logs the number of VCCs obtained for the HA control, whilst for the Ag:HA-Lig coating was drastically lowered (the recovered VCCs being by 20 logs less than control) (Figure 22a), suggesting the gradual and prolonged release of silver ions from the organic-inorganic composite coatings, that interfere with the staphylococcal mature biofilm development. The HA-Lig and Ag:HA-Lig specimens exhibited a similar anti-biofilm activity against the 72h biofilms (reducing by 1.5 to 2.5 logs the VCCs as compared to control) and supporting the hypothesis that Lig improves the implants long-time resistance to staphylococcal colonization. However, even though a more significant decrease of VCCs was observed as compared to control, the increased number of VCCs developed at 72h, as compared to 24 h and 48 h, is pleading for the role of silver ions in the prevention of microbial adherence and for the fact that silver ions are mostly released from the coating in the first 48h of incubation.

The density of the microbial cultures resulting from the multiplication of 24h biofilm embedded cells and measured at 600 nm proved to be much higher than for pure HA coating control (Figure 22b). Conversely, in the case of the 48h and 72h biofilms, the microbial culture density was decreasing in the presence of composite MAPLE coatings compared to the control. Thus, as an effect of the lignin introduction, the hydroxyapatite composite coating (HA-Lig) gained the ability to prevent the development of *S. aureus* biofilm. When silver ions were incorporated (Ag:HA-Lig), the anti-biofilm efficiency slightly increased (Figure 22b).

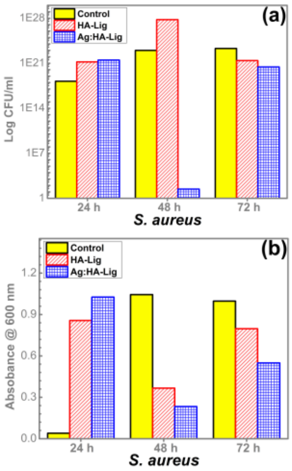

Fig. 22: (a) Number of S. aureus viable cells recovered from the biofilms growing on the tested specimens after 24h, 48h and 72h, respectively; (b) Absorbance values at 600 nm of the S. aureus bacterial biofilm developed on the tested specimens after 24h, 48h and 72h, respectively.

The dynamics of *P. aeruginosa* biofilms on samples were different. The biofilm developed on the pure HA film control specimen had a gradual growth up to 72h (Figure 23a). The assessment of the viable cells harvested from the *P. aeruginosa* biofilms at 24h (Figure 23a) revealed no significant change in the number of viable cells (the quantitative difference being less than one log) developed on the HA-Lig and Ag:HA-Lig specimens, as compared to the pure HA control.

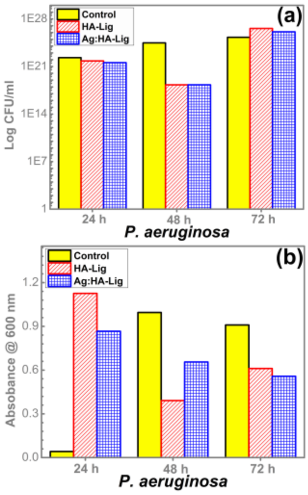

Fig. 23: (a) Number of P. aeruginosa viable cells recovered from the biofilms growing on the tested specimens after 24h, 48h and 72 h, respectively; (b) Absorbance values at 600 nm of the P. aeruginosa bacterial biofilm developed on the tested specimens after 24h, 48h and 72h, respectively.

Contrariwise, some interesting features were observed in the case of 48h biofilms: both HA-Lig and Ag:HA-Lig specimens drastically decreased the number of recovered VCCs (by more than 5 logs) as compared to the pure HA control coating. Both MAPLE coatings showed similar bacteriostatic activity, irrespective of the presence of Ag ions. Therefore, one can suggest that the presence of Lig alone could induce increased antibacterial activity of an implant coating. All specimens showed similar antimicrobial efficiency at 72h. The increased number of VCCs recovered at 72h, as compared with 24h and 48h, is pleading for the efficiency of the tested coatings to delay the biofilm development by preventing the initial microbial adherence, but not to inhibit the formation of the mature biofilm. These results could also be accounted for by the selection of a persistent bacterial population which enters in a state of metabolic latency and stop multiplying, as long as the antimicrobial substances are present, and start to multiply later, when the antimicrobial substances (in the present case Ag ions and Lig) have gone. Similar to *S. aureus* biofilms, the assessment of the total *P. aeruginosa* biofilm development (viable and dead cells) at 24h, quantified by measuring the absorbance at 600 nm (Fig. 23b), showed that HA-Lig and Ag:HA-Lig specimens promoted the biofilm development, as compared to the pure HA control coating. However, at 48h, a drastic decrease in the biofilm density was noticed for the composite coatings, HA-Lig being more efficient than its Ag containing counterpart. This is in good agreement with the above mentioned VCC assays, substantiating the beneficial effect of Lig on the improvement of anti-biofilm properties of the HA coatings. At 72h, both type of organic-inorganic coatings proved equally efficient in preventing the *P. aeruginosa* biofilm cells multiplication (Figure 23b).

VCCs assays indicated that growth of *C. famata* peaked at 72h in the case of pure HA control coating (Figure 24a). Irrespective of the silver ions presence, the number of viable cells recovered from the 24h and 48h *C. famata* biofilms was higher than that obtained for the pure HA control coating, exceeding it with 2 to 5 logs. The HA-Lig and Ag:HA-Lig composite coatings had a strong fungicidal effect against the 72h biofilms. These results could suggest that the HA-Lig and Ag:HA-Lig coatings induce the mature biofilm detachment from the respective surfaces. One may assume that, similar to the case of bacterial biofilms, HA-Lig itself could exhibit a large spectrum of antimicrobial activity.

The quantification of total *C. famata* biofilm by measuring the absorbance at 600 nm evidenced a clear anti-biofilm effect for the two composite coatings, which acted with similar efficiency (Figure 24b).

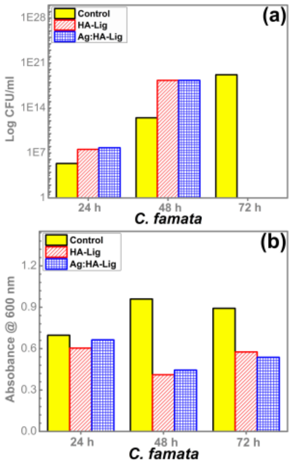

Fig. 24: (a) Number of C. famata viable cells recovered from the biofilms developed on the tested specimens after 24h, 48h and 72h, respectively; (b) Absorbance values at 600 nm of the C. famata fungal biofilm developed on the tested specimens after 24h, 48h and 72h, respectively.

Overall, the biological assays demonstrated that the organic-inorganic lignin-hydroxyapatite composite coatings synthesized by MAPLE could provide an efficient protection against microbial biofilms, without inducing any cytotoxicity towards tested WJ-MSCs.

The role of silver ion as a proficient agent against various bacterial and fungal cultures has been demonstrated [91]. It comes therefore naturally to search for alternate antimicrobial agents, which can work alone or in synergy with renowned antimicrobials.

Following the principles of antibiotic therapy, in which the risk of microbial resistance towards a drug is minimized by using antibiotherapy combinations, we propose a new approach, in which two antimicrobial substances are used to avoid the development of microbial resistance and maximize the cumulative effect. When using two antimicrobial agents, the probability of microbial resistance is the product of probabilities for resistance development used as mono-therapy (when employing singular antimicrobial agents) ($P_{1+2}=P_1xP_2$).

Our results reveal the potential of the natural biopolymer lignin as a reliable antimicrobial agent for implant coatings.

CHAPTER 5. CONCLUSIONS & PERSPECTIVES

5.1. Study I: Biomimetic Apatite

We report the BmAp thin films deposition by Matrix Assisted Pulsed Laser Evaporation (MAPLE) onto titanium substrates.

FTIR spectra of the thin films were found to be highly similar and had an identical signature to the spectrum of the initial powder. The observed shoulders attributed to the HPO_4^{2-} non apatitic ions confirm the preservation of a hydrated phase inside thin films. Raman analyses entirely supported the FTIR results.

Additional AFM investigations identified a typical BmAp morphology after MAPLE transfer. A very limited degradation of the initial nanocrystals was observed, while the obtained films majoritary preserved the composition and structure of the basic powders.

Our results demonstrate that the BmAp biomaterials in the form of thin films show high resemblances to the human hard tissue structures and composition compared to other calcium phosphates and are therefore expected to insure a better functionality to metallic implant coatings.

We conclude that the MAPLE method is capable to maintain the structural fidelity after transfer of biomimetic apatite from a solid frozen target to a nearby substrate, in form of thin film. Characteristic features - such as composition, structure, and adherence - of BmAp thin films can be tailored by optimizing the deposition parameters, demonstrating that the MAPLE technique is a promising alternative for fabrication of metallic implant coatings.

To the best of our knowledge, this is the first report of MAPLE deposition of thin films of poor-crystallized hydrated apatites synthesized by the biomimetic method. We have thus realized and put in evidence the complete transfer of a hydrated, delicate material, proving that its functional groups are present in the deposited films.

5.2. Study II: Ag:HA

We have applied PLD to assemble HA and Ag:HA thin films on the surface of pure Ti and Ti modified by TiO_2 nanotubes substrates.

A quasi-stoichiometric target-to-substrate transfer was ascertained by EDS, whilst the restoration of the crystalline status after post-deposition heat-treatment performed at 500 °C in water vapors for six hours was confirmed by the FTIR and XRD analyses. Thus, benefic effects on the long term stability of these films in biological fluids should be expected. We have shown by AFM that Ag:HA thin films exhibit nanostructured topography which is prone to allow a better biointegration of the implant.

Dedicated cytotoxicity tests of glass control, Ti substrate, $nTiO_2$/Ti substrate, and Ag:HA/$nTiO_2$/Ti coating have been conducted. The results were at the basis of our choice for conducting the microbiological antifungal testing on the crystalline Ag:HA thin films deposited on Ti modified by TiO_2 nanotubes substrates. The tests were conducted against two common pathogenic fungal strains, *Candida albicans* and *Aspergillus niger*. The biological assays demonstrated the high antifungal efficiency of heat-treated Ag:HA thin films deposited on Ti modified by TiO_2 nanotubes substrates which completely exterminate *Candida albicans* and radically reduce the *Aspergillus niger* number of colonies.

Our conclusion is that the deposition by PLD of Ag:HA thin films on Ti modified with TiO_2 nanotubes substrates followed by a heat treatment at 500 °C in water vapors for six hours, allows for the fabrication of efficient shield barriers against adherence and contamination by pathogenic fungi.

5.3. Study III: Ag-Lig:HA

We report on the transfer by Matrix-Assisted Pulsed Laser Evaporation of a large macromolecule of undefined molecular weight - organosolv lignin (Lig) - embedded in a hydroxyapatite film matrix. When silver was incorporated into HA lattice, it yielded another composite, Ag:HA-Lig. The promptness and accuracy of the MAPLE technique was demonstrated for deposition of such delicate, yet bulky material, as suggested by EDS and proved by XPS and FTIR results. The obtained nanocomposites were non-cytotoxic, supporting a normal development and promoting the growth of the adhered human mesenchymal cells. The microbiological assays showed that the coated composite secured a prolonged release of silver ions, being protective both against the initial phase of microbial colonization and the mature biofilm development. The lignin addition boosted the anti-microbial activity of HA doped with silver ions against both bacterial and fungal biofilms. An implant surface modified in such a manner could host osteogenic cell proliferation while shielding from bacteria and fungi, thus facilitating a safe osteointegration of the medical device.

REFERENCES

[1] V. Nelea, M. Jelinek M, I.N. Mihailescu, Biomaterials: new issues and breakthroughs for biomedical applications, in: R. Eason (Ed), Pulsed Laser Deposition of thin films: applications-lead growth of functional materials, Wiley & Sons, 2006.

[2] S.V. Dorozhkin, Nanodimensional and Nanocrystalline Apatites and Other Calcium Orthophosphates in Biomedical Engineering, Biology and Medicine. Materials 2 (2009) 1975–2045.

[3] I.N. Mihailescu, C. Ristoscu, A. Bigi, I. Mayer, Advanced biomimetic implants based on nanostructured coatings synthesized by pulsed laser technologies, in: A. Miotello, P.M. Ossi (Eds.), Laser-Surface Interactions for New Materials Production Tailoring Structure and Properties, Springer Series in Materials Science, 2010.

[4] B. Leon, J.A. Jansen, Thin calcium phosphates coatings for medical implants, Materials Science Chemistry, Springer, 2009.

[5] L. Duta, F.N. Oktar, G.E. Stan, G. Popescu-Pelin, N. Serban, C. Luculescu, I.N. Mihailescu, Novel doped hydroxyapatite thin films obtained by Pulsed Laser Deposition, Appl. Surf. Sci. 265 (2013) 41–49.

[6] C. Rey, A. Hina, A. Tofighi, M.J. Glimcher, Maturation of poorly crystalline apatites: chemical and structural aspects in vivo and in vitro, Cell Mater. 5-4 (1995) 345–356.

[7] D. Eichert, C. Drouet, H. Sfihi, C. Rey, C. Combes, Nanocrystalline apatite-based biomaterials: synthesis, processing and characterization, in: B.J. Kendall (Ed), Nanocrystalline apatite-based biomaterials: synthesis, processing and characterization, Biomaterials Research Advances, Nova Science Publishers, 2007.

[8] P. Habibovic, F. Barrere, C.A. van Blitterswijk, K. de Groot, P. Layrolle, Biomimetic hydroxyapatite coating on metal implants, J. Am. Ceram. Soc. 85 (2002) 517–522.

[9] R.Z. Le Geros, Biodegradation and Bioresorption of calcium phosphate ceramics, Clin. Mater. 14 (1993) 65–88.

[10] B.R. Ringeisen, J. Callahan, P.K. Wu, A. Pique, B. Spargo, R.A McGill, M. Bucaro, H. Kim, D.M. Bubb, D.B. Chrisey, Novel Laser-Based Deposition of Active Protein Thin Films, Langmuir 17 (2001) 3472–3479.

[11] R. Cristescu, I.N. Mihailescu, M. Jelinek, D.B. Chrisey, Functionalized Thin Films & Structures Obtained by Novel Laser Processing Issues, in: R. Kassing, P. Petkov, W. Kulisch, C. Popov (Eds.), Functionalized Thin Films & Structures Obtained by Novel Laser Processing Issues, NATO Science Series by Springer, Series II: Mathematics, Physics and Chemistry 223 (2006) 211–226.

[12] A. Pique, Deposition of Polymers and Biomaterials Using the Matrix-Assisted Pulsed Evaporation (MAPLE) Process, in: R. Eason (Ed), Deposition of Polymers and Biomaterials Using the Matrix-Assisted Pulsed Evaporation (MAPLE) Process, Wiley-Interscience, 2007.

[13] I.N. Mihailescu, E. Gyorgy, Pulsed laser deposition: an overview, 4-th international commission for optics (ico) book in: International trends in optics and photonics, Ed. T. Asakura (ico president), 1999, pp. 201-214.

[14]. T.R. Rautray, R. Narayanan, T.-Y. Kwon, K.-H. Kim, Surface modification of titanium and titanium alloys by ion implantation, J. Biomed. Mater. Res. B 93B (2010) 581–591.

[15]. A. Kar, K.S. Raja, M. Misra, Electrodeposition of hydroxyapatite onto nanotubular TiO_2

for implant applications, Surf. Coat. Technol. 201 (2006) 3723–3731.

[16].V. Kotharu, R. Nagumothu, C. Bose Arumugam, M. Veerappan, S. Sankaran, M. A. Davoodbasha, T. Nooruddin, Fabrication of corrosion resistant, bioactive and antibacterial silver substituted hydroxyapatite/titania composite coating on cp Ti, Ceram. Int. 38 (2012) 731–740.

[17]. Y.L. Jeyachandran, Sa.K. Narayandass, D. Mangalaraj, C.Y. Bao, W. Li, Y.M. Liao, C.L. Zhang, L.Y. Xiao, W.C. Chen, A study on bacterial attachment on titanium and hydroxyapatite based films, Surf. Coat. Technol. 201 (2006) 3462–3474.

[18].J.M. Macak, H. Tsuchiya, A. Ghicov, K. Yasuda, R. Hahn, S. Bauer, P. Schmuki, TiO_2 nanotubes: Self-organized electrochemical formation, properties and applications, Curr. Opin. Solid State Mater. Sci. 11 (2007) 3–18.

[19]. N.F. Fahim, M. F. Morks, T. Sekino, Electrochemical synthesis of silica-doped high aspect-ratio titania nanotubes as nanobioceramics for implant applications, Electrochim. Acta 54 (2009) 3255–3269.

[20]. G.C. Smith, L. Chamberlain, L. Faxius, G.W. Johnston, S. Jin, L.M. Bjursten, Soft tissue response to titanium dioxide nanotube modified implants, Acta Biomater. 7 (2011) 3209–3215.

[21]. N. Torres, S. Oh, M. Appleford, D.D. Dean, J.H. Jorgensen, J.L. Ong, C. Mauli Agrawal, G. Mani, Stability of antibacterial self-assembled monolayers on hydroxyapatite, Acta Biomater. 6 (2010) 3242–3255.

[22]. M. Gajbhiye, J. Kesharwani, A. Ingle, A. Gade, M. Rai, Fungus-mediated synthesis of silver nanoparticles and their activity against pathogenic fungi in combination with fluconazole, Nanomedicine 5 (2009) 382–386.

[23]. G.A. Fielding, M. Roy, A. Bandyopadhyay, S. Bose, Antibacterial and biological characteristics of silver containing and strontium doped plasma sprayed hydroxyapatite coatings, Acta Biomater. 8 (2012) 3144–3152.

[24]. N.A. Trujillo, R.A. Oldinski, H. Ma, J.D. Bryers, J.D. Williams, K.C. Popat, Antibacterial effects of silver-doped hydroxyapatite thin films sputter deposited on titanium, Mater. Sci. Eng. C 32 (2012) 2135–2144.

[25]. A. Ewald, D. Hösel, S. Patel, L.M. Grover, J.E. Barralet, U. Gbureck, Silver-doped calcium phosphate cements with antimicrobial activity, Acta Biomater. 7 (2011) 4064–4070.

[26]. W. Chen, Y. Liu, H. S. Courtney, M. Bettenga, C.M. Agrawal, J.D. Bumgardner, J.L. Ong, In vitro anti-bacterial and biological properties of magnetron co-sputtered silver-containing hydroxyapatite coating, Biomaterials 27 (2006) 5512–5517.

[27]. A. Simchi, E. Tamjid, F. Pishbin, A.R. Boccaccini, Recent progress in inorganic and composite coatings with bactericidal capability for orthopaedic applications, Nanomedicine 7 (2011) 22−39.

[28]. Y. Huang, L. Song, X. Liu, Y. Xiao, Y. Wu, J. Chen, F. Wu, Z. Gu, Hydroxyapatite coatings deposited by liquid precursor plasma spraying: controlled dense and porous microstructures and osteoblastic cell responses, Biofabrication 2 (2010) 045003.

[29]. L.E. Sima, G.E. Stan, C.O. Morosanu, A. Melinescu, A. Ianculescu, R. Melinte, J. Neamtu, S.M. Petrescu, Differentiation of mesenchymal stem cells onto highly adherent radio frequency-sputtered carbonated hydroxylapatite thin films, J. Biomed. Mater. Res. A 95A (2010) 1203–1214.

[30]. V. Nelea, M. Jelinek, I.N. Mihailescu, Chapter 18: Biomaterials: New issues and breakthroughs for biomedical applications, in: Pulsed laser deposition of thin films: Applications-lead growth of functional materials, John Wiley & Sons, 2006, pp. 421–456.

[31]. G. Socol, M. Socol, L. Sima, S. Petrescu, M. Enculescu, F. Sima, M. Miroiu, G. Popescu-Pelin, N. Stefan, R. Cristescu, C.N. Mihailescu, A. Stanculescu, C. Sutan, I.N. Mihailescu, Combinatorial pulsed laser deposition of Ag-containing calcium phosphate coatings, Dig. J. Nanomater. Biostructr. 7 (2012) 563–576.

[32]. T.F. Stoica, C. Morosanu, A. Slav, T. Stoica, P. Osiceanu, C. Anastasescu, M. Gartner, M. Zaharescu, Hydroxyapatite films obtained by sol–gel and sputtering, Thin Solid Films 516 (2008) 8112–8116.

[33]. M.S. Djošić, V. Panić, J. Stojanović, M. Mitrić, V.B. Mišković-Stanković, The effect of applied current density on the surface morphology of deposited calcium phosphate coatings on titanium, Colloids Surf. A 400 (2012) 36–43.

[34]. S. Eraković, Dj. Veljović, P.N. Diouf, T. Stevanović, M. Mitrić, Dj. Janaćković, I. Z. Matić, Z.D. Juranić, V.B. Mišković-Stanković, The effect of lignin on the structure and characteristics of composite coatings electrodeposited on titanium, Prog. Org. Coat. 75 (2012) 275–283.

[35]. S. Eraković, A. Janković, Dj. Veljović, E. Palcevskis, M. Mitrić, T. Stevanović, Dj. Janaćković, V.Mišković-Stanković, Corrosion stability and bioactivity in simulated body fluid of silver/hydroxyapatite and silver/hydroxyapatite/lignin coatings on titanium obtained by electrophoretic deposition, J. Phys. Chem. B 117 (2013) 1633–1643.

[36]. Cazacu G, Capraru M, Popa VI. Advances concerning Lignin utilization in new materials. In: Thomas S, Visak PM, Mathew AP, editors. Advances in Natural Polymers: Composites and Nanocomposites. New York: Springer Heidelberg; 2013. pp. 255–312. DOI: 10.1007/978-3-642-20940-6_8.

[37] Santillán MJ, Quaranta NE, Boccaccini AR. Titania and titania–silver nanocomposite coatings grown by electrophoretic deposition from aqueous suspensions. Surf. Coat. Technol. 2010;205:2562–71. DOI: 10.1016/j.surfcoat.2010.10.001.

[38] Pique A. Deposition of polymers and biomaterials using the Matrix-Assisted Pulsed Evaporation (MAPLE) process. In: R Eason, editor. Pulsed Laser Deposition of Thin Films. Applications-Led Growth of Functional Materials. New Jersey: Wiley Interscience; 2007. pp. 63–84. DOI: 10.1002/9780470052129.ch3.

[39] Eraković S, Janković A, Ristoscu C, Duta L, Serban N, Visan A, Mihailescu IN, Stan GE, Socol M, Iordache O, Dumitrescu I, Luculescu CR, Janaćković Dj, Miškovic-Stanković V. Antifungal activity of Ag:hydroxyapatite thin films synthesized by pulsed laser deposition on Ti and Ti modified by TiO_2 nanotubes substrates. Appl. Surf. Sci. 2014;293:37– 45. DOI: 10.1016/j.apsusc.2013.12.029.

[40] D. Grossin, S. Rollin-Martinet, C. Estournes, F. Rossignol, E. Champion, C. Combes, C. Rey, C. Geoffroy, C. Drouet, Biomimetic apatite sintered at very low temperature by spark plasma sintering: Physico-chemistry an microstructure aspects, Acta Biomater 6 (2010) 577–585.

[41]. D. Eichert, C. Drouet, H. Sfihi, C. Rey, C. Combes, Nanocrystalline apatite-based

biomaterials: synthesis, processing and characterization, in: B.J. Kendall (Ed), Nanocrystalline apatite-based biomaterials: synthesis, processing and characterization, Biomaterials Research Advances, Nova Science Publishers, 2007.

[42]. B.C. Riggs, A.D. Dias, N.R. Schiele, R. Cristescu, Y. Huang, D.T. Corr, D.B. Chrisey, Matrix-Assisted Pulsed Laser Methods for Biofabrication, EMRS Bul. 36 (2011) 1043–1050.

[43]. G. Socol, M. Socol, L. Sima, S. Petrescu, M. Enculescu, F. Sima, M. Miroiu, G. Popescu-Pelin, N. Stefan, R. Cristescu, C.N. Mihailescu, A. Stanculescu, C. Sutan, I.N. Mihailescu, Combinatorial pulsed laser deposition of Ag-containing calcium phosphate coatings, Dig. J. Nanomater. Biostructr. 7 (2012) 563–576.

[44]. G. Charlot, Chimie analytique quantitative, Masson Paris, 1974.

[45]. J. Li, K. Hirota, T. Goto, H.Yumoto, Y. Miyake, T. Ichikawa, Biofilm formation of Candida albicans on implant overdenture materials and its removal, J. Dent. 40 (2012) 686–692.

[46]. V.L. Laurel, P.A. Meier, A. Astorga, D. Dolan, R. Brockett,M.G. Rinaldi, Pseudoepidemic of Aspergillus niger Infections Traced to Specimen Contamination in the Microbiology Laboratory, J. Clin. Microbiol. 37(5) (1999) 1612–1616.

[47]. Grumezescu AM, Holban AM, Andronescu E, Mogosanu GD, Vasile BS, Chifiriuc MC, Lazar V, Andrei E, Constantinescu A, Maniu H. Anionic polymers and 10 nm Fe_3O_4@UA wound dressings support human foetal stem cells normal development and exhibit great antimicrobial properties. Int. J. Pharm. 2013; DOI: 10.1016/j.ijpharm.2013.08.026.

[48]. A. Boskey, Bone mineral crystal size, Osteoporos Int. 14 (2003) S16–S21.

[49]. S.L. Rowles, Studies on non-stoichiometric apatites, in: R.W. Fearnhead, M.W. Stack (Eds.), Studies on non-stoichiometric apatites, Tooth Enamel Proc. Int. Symp., Bristol John Wright & Sons, 1965.

[50] N. Van Decandelaere, C. Rey, C. Drouet, Biomimetic apatite-based biomaterials: on the critical impact of synthesis and post-synthesis parameters, J. Mater. Sci: Mater. Med. 23 (2012) 2593–2606.

[51] C. Rey, E. Strawich, M.J. Glimcher, Non-apatitic environments in Ca-P biominerals; implications in reactivity of the mineral phase and its interactions with organic matrix constituents, in: D. Allemand, J.P. Cuif (Eds.), Non-apatitic environments in Ca-P biominerals; implications in reactivity of the mineral phase and its interactions with organic matrix constituents, Rev. Mineral. Geochem. 55–64 (1994).

[52] R. Cristescu, C. Popescu, G. Socol, I. Iordache, I.N. Mihailescu, D.E. Mihaiescu, A.M. Grumezescu, A. Andronie, I. Stamatin, C. Chifiriuc, C. Bleotu, C. Saviuc, M. Popa, D.B. Chrisey, Magnetic Core/Shell Nanoparticle Thin Films Deposited By MAPLE: Investigation By Chemical, Morphological And In Vitro Biological Assays, Appl. Surf. Sci. 258 (2012) 9250–9255.

[53]. G. Mendonça, D.B.S. Mendonça, L.G.P. Simões, A.L. Aráujo, E.R. Leite, W.R. Duarte, F.J.L. Aragão, L.F. Cooper, The effects of implant surface nanoscale features on osteoblast specific gene expression, Biomaterials 30 (2009) 4053–4062.

[54]. T. Raimondo, S. Puckett, T.J. Webster, Greater osteoblast and endothelial cell adhesion on nanostructured polyethylene and titanium, Int. J. Nanomedicine 5 (2010) 647–652.

[55]. S. Okada, H. Ito, A. Nagai, J. Komotori, H. Imai, Adhesion of osteoblast-like cells on nanostructured hydroxyapatite, Acta Biomater. 6 (2010) 591–597.

[56]. P.V. Tuttle, A.E. Rundell, T.J. Webster, Influence of biologically inspired nanometer surface roughness on antigen-antibody interactions for immunoassay-biosensor applications, Int. J. Nanomedicine 1 (2006) 497–505.

[57]. G.E. Stan, A.C. Popescu, I.N. Mihailescu, D.A. Marcov, R.C. Mustata, L.E. Sima, S.M. Petrescu, A. Ianculescu, R. Trusca, C.O. Morosanu, On the bioactivity of adherent bioglass thin films synthesized by magnetron sputtering techniques,Thin Solid Films 518 (2010) 5955–5964.

[58]. Particulates in pulsed laser deposition: Formation mechanisms and possible approaches to their elimination, I.N. Mihailescu, V.S. Teodorescu, E. Gyorgy, C. Ristoscu, R. Cristescu, Proceedings of SPIE - The International Society for Optical Engineering 4762, pp. 64-74, 2002.

[59]. M. Sygnatowicz, A. Tiwari, Controlled synthesis of hydroxyapatite-based coatings for biomedical application, Mater. Sci. Eng. C 29 (2009) 1071–1076; doi: 10.1016/j.msec.2008.08.036.

[60]. R. Narayanan, T.-Y. Kwon, K.-H. Kim, Direct nanocrystalline hydroxyapatite formation on titanium from ultrasonated electrochemical bath at physiological, Mater. Sci. Eng. C 28 (2008) 1265–1270; doi: 10.1016/j.msec.2007.11.009

[61]. G. Socrates, Infrared and Raman Characteristic Group Frequencies—Tables and Charts, 3rd ed., John Wiley & Sons Ltd., 2004.

[62]. A. Antonakosa, E. Liarokapis, T. Leventouri, Micro-Raman and FTIR studies of synthetic and natural apatites, Biomaterials 28 (2007) 3043–3054.

[63]. M. Markovic, B.O. Fowler, M.S. Tung, Preparation and comprehensive characterization of a calcium hydroxyapatite reference material, J. Res. Natl. Inst. Stand. Technol. 109 (2004) 553–568.

[64]. J.D. Pasteris, B. Wopenka, J.J. Freeman, K. Rogers, E. Valsami-Jones, J.A.M. van der Houwen, M.J. Silva, Lack of OH in nanocrystalline apatite as a function of degree of atomic order: implications for bone and biomaterials, Biomaterials 25 (2004) 229–238.

[65]. R.A. Young, D.W. Holcomb, Role of acid phosphate in hydroxyapatite lattice expansion, Calcif. Tissue Int. 36 (1984) 60–63.

[66]. G. Spence, S. Phillips, C. Campion, R. Brooks, N. Rushto, Bone formation in a carbonate-substituted hydroxyapatite implant is inhibited by zoledronate: the importance of bioresorption to osteoconduction, J. Bone Joint. Surg. Br. 90 (2008) 1635–1640.

[67]. M.Z. Hu, P. Lai, M.S. Bhuiyan, C. Tsouris, B. Gu, P. Paranthaman, J. Gabitto, L. Harrison, Synthesis and characterization of anodized titanium-oxide nanotube arrays, J. Mater. Sci. 44 (2009) 2820–2827.

[68]. H. Khandelwal, G. Singh, K. Agrawal, S. Prakash, R.D. Agarwal, Characterization of hydroxyapatite coating by pulse laser deposition technique on stainless steel 316 L by varying laser energy, Appl. Surf. Sci. 265 (2013) 30– 35; doi: 10.1016/j.apsusc.2012.10.072.

[69]. C.S. Ciobanu, S.L. Iconaru, P. Le Coustumer, L.V. Constantin, D. Predoi, Antibacterial activity of silver-doped hydroxyapatite nanoparticles against gram-positive and gram-negative bacteria, Nanoscale Res. Lett. 7 (2012) 324, doi:10.1186/1556-276X-7-324.

[70]. A. Patterson, The Scherrer formula for X-ray particle size determination, Phys. Rev. 56 (1939) 978–982.
[71]. J. Li, K. Hirota, T. Goto, H.Yumoto, Y. Miyake, T. Ichikawa, Biofilm formation of Candida albicans on implant overdenture materials and its removal, J. Dent. 40 (2012) 686–692.
[72]. Eraković S, Janković A, Veljović Dj, Palcevskis E, Mitrić M, Stevanovic T, Janaćković Dj, Mišković-Stanković V. Corrosion stability and bioactivity in simulated body fluid of silver/hydroxyapatite and silver/hydroxyapatite/lignin coatings on titanium obtained by electrophoretic deposition. J. Phys. Chem. B. 2013;117:1633−43. DOI: 10.1021/jp305252a.
[73]. Cristescu R, Popescu C, Popescu AC, Grigorescu S, Duta L, Mihailescu IN, Caraene G, Albulescu R, Albulescu L, Andronie A, Stamatin I, Ionescu A, Mihaiescu D, Buruiana T, Chrisey DB. Functionalized polyvinyl alcohol derivatives thin films for controlled drug release and targeting systems: MAPLE deposition and morphological, chemical and in vitro characterization. Appl. Surf. Sci. 2009;255:5600–4. DOI: 10.1016/j.apsusc.2008.09.047.

[74]. Cristescu R, Popescu C, Socol G, Visan A, Mihailescu IN, Gittard SD, Miller PR, Martin TN, Narayan RJ, Andronie A, Stamatin I, Chrisey DB. Deposition of antibacterial of poly(1,3-bis-(p-carboxyphenoxy propane)-co-(sebacic anhydride)) 20:80/gentamicin sulfate composite coatings by MAPLE. Appl. Surf. Sci. 2011;257:5287–92. DOI:10.1016/j.apsusc.2010.11.141.

[75]. Eraković S, Janković A, Ristoscu C, Duta L, Serban N, Visan A, Mihailescu IN, Stan GE, Socol M, Iordache O, Dumitrescu I, Luculescu CR, Janaćković Dj, Miškovic-Stanković V. Antifungal activity of Ag:hydroxyapatite thin films synthesized by pulsed laser deposition on Ti and Ti modified by TiO_2 nanotubes substrates. Appl. Surf. Sci. 2014;293:37– 45. DOI: 10.1016/j.apsusc.2013.12.029.
[76]. Cros A. Charging effects in X-ray photoelectron spectroscopy. J. Electron. Spectrosc. Relat. Phenom. 1992;59:1–14. DOI: 10.1016/0368-2048(92)85008-U.

[77] Johansson LS, Campbell JM. Reproducible XPS on biopolymers: cellulose studies. Surf. Interface Anal. 2004;36:1018–22. DOI: 10.1002/sia.1827.

[78] Guo JB, Tao ZY, Luo XG. Analysis of bamboo lignin with FTIR and XPS. Acta Chim. Sin. 2005;63:1536–40. http://sioc-journal.cn/Jwk_hxxb/EN/abstract/abstract335917.shtml

[79] Kalaskar DM, Ulijn RV, Gough JE, Alexander MR, Scurr DJ, Sampson WW, Eichhorn SJ. Characterisation of amino acid modified cellulose surfaces using ToF-SIMS and XPS. Cellulose. 2010;17:747–56. DOI: 10.1007/s10570-010-9413-y.

[80]. Markovic M, Fowler BO, Tung MS. Preparation and comprehensive characterization of a calcium hydroxyapatite reference material. J. Res. Natl. Inst. Stand. Technol. 2004;109:553–68. DOI: 10.6028/jres.109.042.
[81]. Arumugam SK, Sastry TP, Sreedhar B, Mandal AB. One step synthesis of silver nanorods by autoreduction of aqueous silver ions with hydroxyapatite: An inorganic-inorganic hybrid nanocomposite. J. Biomed. Mater. Res. 2007;80:391–8. DOI: 10.1002/jbm.a.30895.

[82] Kline LM, Hayes DG, Womac AR, Labbé N. Simplified determination of lignin content in hard and soft woods via UV-spectrophotometric analysis of biomass dissolved in ionic liquids. BioResources. 2010;5:66–1383. http://www.ncsu.edu/bioresources/BioRes_05_3.html.

[83] Rana R, Langenfeld-Heyser R, Finkeldey R, Polle A. FTIR spectroscopy, chemical and histochemical characterisation of wood and lignin of five tropical timber wood species of the family of Dipterocarpaceae. Wood Sci. Technol. 2010;44:225–42. DOI 10.1007/s00226-009-0281-2.

[84] Popescu CM, Popescu MC, Singurel G, Vasile C, Argyropoulos DS, Willfor S. Spectral characterization of eucalyptus wood. Appl. Spectrosc. 2007;61:1168–77. DOI: 10.1366/000370207782597076.

[85]. Grumezescu AM, Holban AM, Andronescu E, Mogosanu GD, Vasile BS, Chifiriuc MC, Lazar V, Andrei E, Constantinescu A, Maniu H. Anionic polymers and 10 nm Fe_3O_4@UA wound dressings support human foetal stem cells normal development and exhibit great antimicrobial properties. Int. J. Pharm. 2013; DOI: 10.1016/j.ijpharm.2013.08.026.

[86] Bianco P, Riminucci M, Gronthos S, Robey PG. Bone marrow stromal stem cells: nature, biology, and potential applications. Stem Cells. 2001;19:180–92. DOI: 10.1634/stemcells.19-3-180.

[87] Forte G, Franzese O, Pagliari S, Pagliari F, Di Francesco AM, Cossa P, Laudisi A, Fiaccavento R, Minieri M, Bonmassar E, Di Nardo P. Interfacing Sca-1^{pos} mesenchymal stem cells with biocompatible scaffolds with different chemical composition and geometry. J. Biomed. Biotechnol. 2009; DOI: 10.1155/2009/910610.

[88] Zhao L, Chu PK, Zhang Y, Wu Z. Antibacterial coatings on titanium implants. J. Biomed. Mater. Res. B–Appl Biomater. 2009;91:470–80. DOI: 10.1002/jbm.b.31463.

[89] Schmidmaier G, Lucke M, Wildemann B, Haas NP, Raschke M. Prophylaxis and treatment of implant-related infections by antibiotic-coated implants: a review. Injury. 2006;37:S105–12. DOI: 10.1016/j.injury.2006.04.016.

[90] Agnihotri S, Mukherji S, Mukherji S. Immobilized silver nanoparticles enhance contact killing and show highest efficacy: elucidation of the mechanism of bactericidal action of silver. Nanoscale. 2013;5:7328–40. DOI: 10.1039/C3NR00024A.

[91] Arumugam SK, Sastry TP, Sreedhar B, Mandal AB. One step synthesis of silver nanorods by autoreduction of aqueous silver ions with hydroxyapatite: An inorganic-inorganic hybrid nanocomposite. J. Biomed. Mater. Res. 2007;80:391–8. DOI: 10.1002/jbm.a.30895.

LIST OF CONTRIBUTION

1.R. Cristescu, A.V. Surdu, A.M. Grumezescu, A.E. Oprea, R. Trusca, O. Vasile, G. Dorcioman, **A.Visan**, G. Socol, I.N. Mihailescu, D. Mihaiescu, M. Enculescu, M.C. Chifiriuc, R.D. Boehm, R.J. Narayan, D.B. Chrisey,(2015),Microbial colonization of biopolymeric thin films containing natural compounds and antibiotics fabricated by MAPLE, Applied Surface Science, 336, Pages 234-239. **IF (2013) =2.538**

2.A. Janković, S. Eraković, C. Ristoscu, N. Mihailescu (Serban), L. Duta, **A.Visan**, G.E. Stan, A.C. Popa, M.A. Husanu, C.R. Luculescu, V.V. Srdić, Dj. Janaćković, V. Mišković-Stanković, C. Bleotu, M.C. Chifiriuc, I.N. Mihailescu,(2014),Structural and biological evaluation of lignin addition to simple and silver doped hydroxyapatite thin films synthesized by matrix-assisted pulsed laser evaporation", Journal of Materials Science: Materials in Medicine, (1):5333. doi: 10.1007/s10856-014-5333-y **IF (2013) =2.379**

3.S. Eraković, A. Janković, C. Ristoscu, L. Duta, N. Serban, **A.Visan**, I.N. Mihailescu, G.E. Stan, M. Socol, O. Iordache, I. Dumitrescu, C.R. Luculescu, Dj. Janaćković, V. Miškovic-Stanković, (2014),Antifungal activity of Ag:hydroxyapatite thin films synthesized by pulsed laser deposition on Ti and Ti modified by TiO2 nanotubes substrates", Applied Surface Science, 293, Pages 37-45. **IF (2013) =2.538**

4. **A.Visan**, D. Grossin, N. Stefan, L. Duta, F.M. Miroiu, G.E. Stan, M. Sopronyi, C. Luculescu, M. Freche, O. Marsan, C. Charvilat, S. Ciuca, I.N. Mihailescu,(2014), "Biomimetic nanocrystalline apatite coatings synthesized by Matrix Assisted Pulsed Laser Evaporation for medical applications", Materials Science and Engineering B, 181, 56-63. **IF (2013) =2.122**

5. Socol, G., Preda, N., Socol, M., Sima, L., Luculescu, C.R., Sima, F., Miroiu, M., Axente, E., **A.Visan**., Stefan, N., Cristescu, R., Dorcioman, G., Stanculescu, A., Radulescu, L., Mihailescu, I.N., (2013) "MAPLE deposition of PLGA micro-and nanoparticles embedded into polymeric coatings", Digest Journal of Nanomaterials and Biostructures, 8 (2), pp. 621-630 **IF(2013)=1.123**

6.R.Cristescu, C. Popescu, G. Socol, **A.Visan**, I.N. Mihailescu, S.D. Gittard, P.R. Miller, T.N. Martin, R.J. Narayan, A. Andronie, I. Stamatin, D.B. Chrisey, (2011), Deposition of antibacterial of poly(1,3-bis-(p-carboxyphenoxy propane)-co-(sebacic anhydride)) 20:80/gentamicin sulfate composite coatings by MAPLE" , Applied Surface Science, 257 5287–5292. **IF(2011)= 2.103**

7.F.M. Miroiu , G. Socol, **A.Visan**, N. Stefan, D. Craciun, V. Craciun, G. Dorcioman, I.N. Mihailescu, L.E. Sima, S.M. Petrescu, A. Andronie, I. Stamatin, S. Moga and C. Ducu, (2010),"Composite biocompatible hydroxyapatite–silk fibroin coatings for medical implants obtained by Matrix Assisted Pulsed Laser Evaporation", Materials Science and Engineering B, 169, 151–158. **IF(2010)= 1.518**

INTERNATIONAL CONFERENCES

1. Autori, Numele doctorandului, autori (2005) Titlul conferintei, Locatia, Data/Perioada,

1. **A.Visan**, M. Miroiu, N. Stefan, C. Nita, G. Dorcioman, I. Zgura, O.L. Rasoaga, C.S. Breazu, A. Stanculescu, R. Cristescu, G. Socol, I.N. Mihailescu(2014),Matrix Assisted Pulsed Laser Evaporation vs. Dip Coating techniques for fabrication of biodegradable polymer thin films with medical applications,International Conference"MODERN LASER APPLICATIONS"Fourth Edition, 19-23 Mai, Bran,Romania,prezentare poster P18

2. N. Stefan, F.M. Miroiu, **A.Visan**, O.L. Rasoga, I. Zgura, A. Stanculescu, G. Socol(2014),Biodegradable silk fibroin/poly(sebacic acid) diacetoxy terminated composite coatings obtained by matrix assisted pulsed laser evaporation,(2014)International Conference"MODERN LASER APPLICATIONS"Fourth Edition, 19-23 Mai, Bran,Romania,poster P20

3. **A.Visan**,D. Grossin, N. Stefan, L. Duta, F. M. Miroiu, M. Sopronyi, F. Miculescu, M. Freche, C. Charvilat, O, Marsan, S. Ciuca, I.N. Mihailescu(2014),Matrix Assisted Pulsed Laser Evaporation synthesis of biomimetic nanocrystalline apatite coatings with applications in medicine,International Conference"MODERN LASER APPLICATIONS"Fourth Edition, 19-23 Mai, Bran,Romania,16.00 –16.15 Prezentare orala: O5

4. **A.Visan**, D. Grossin, N. Stefan, L. Duta, F.M. Miroiu, G.E. Stan, M. Sopronyi, C. Luculescu, M. Freche, O. Marsan, C. Charvilat, S. Ciuca, I.N. Mihailescu(2014),Matrix Assisted Pulsed Laser Evaporation synthesis of biomimetic nanocrystalline apatite coatings for biomedical applications,EMRS 2014, Symposium : J Laser interaction with advanced materials: fundamentals and applications, Lille,France , May 26-30),Prezentare Poster, 27mai, cod panou: JP.VIII 5

5. **A.Visan**, M. Miroiu, N. Stefan, C. Nita, G. Dorcioman, I. Zgura, O.L. Rasoaga, C.S. Breazu, A. Stanculescu, R. Cristescu, G. Socol, I.N. Mihailescu(2014),Fabrication of biodegradable polycaprolactone -polyethylene glycol composite coatings by Matrix Assisted Pulsed Laser Evaporation and Dip Coatings,EMRS 2014, Symposium : J Laser interaction with advanced materials: fundamentals and applications, Lille,France , May 26-30),Prezentare Poster, 27mai, ,cod panou: JP.VIII 4

6. M. Sopronyi, C. Nita, V. Grumezescu, O.L. Rasoga, N. Stefan, C.S. Breazu, M. Socol, I. Zgura, **A.Visan**, G. Popescu-Pelin, A. Stanculescu, I.N. Mihailescu, G. Socol(2014)Deposition and characterization of polyethylene glycol/poly(3-hydroxybutyrate-co-3-hydroxyvalerate) blends,EMRS 2014, Symposium : J Laser interaction with advanced materials: fundamentals and applications, Lille,France , May 26-30),Prezentare Poster, 27mai ,cod panou: JP.VIII 9

7. C.Nita, E. Axente, F. Sima, I. Iordache, R. Cristescu, **A.Visan**, I. Zgura, O.L. Rasoaga, C.S. Breazu, A. Stanculescu, G. Socol(2014)Comparative study on the deposition of biodegradable PCL/PLA blend coatings,EMRS 2014, Symposium : J Laser interaction with advanced materials: fundamentals and applications, Lille,France , May 26-30),Prezentare

Poster, 27mai,ora 16,cod panou: JP.VIII 37

8. F.M. Miroiu, N. Stefan, **A.Visan**, O.L. Rasoga, I. Zgura, C.Nita, A. Stanculescu, G. Dorcioman, R. Cristescu, I. N. Mihailescu, G. Socol(2014),Biodegradable Silk Fibroin/Poly(3-Hydroxy-Butyric Acid-Co-3-Hydroxy-Valeric Acid) composite coatings obtained by MAPLE and dip-coating methods,EMRS 2014, Symposium : J Laser interaction with advanced materials: fundamentals and applications, Lille,France , May 26-30),Prezentare Poster,

9. G. Popescu-Pelin, E. Axente, F. Sima, I. Iordache, C. Nita, **A.Visan**, I. Zgura, O.L. Rasoaga, C.S. Breazu, A. Stanculescu, G. Socol, I.N. Mihailescu(2014),,Comparative study on the deposition of polymeric coatings based on PCL/PLGA blends,EMRS 2014, Symposium : J Laser interaction with advanced materials: fundamentals and applications, Lille,France , May 26-30),Prezentare Poster, cod panou: JP. VIII 8

10. G. Socol, V. Grumezescu, C. Nita, G. Dorcioman, N. Stefan, M. Miroiu, I. Zgura, M. Socol, **A.Visan**, G. Popescu-Pelin, R. Cristescu, O. Rasoga, C.S. Breazu, A. Stanculescu(2014),,Deposition and characterization of calcium phosphates/poly(3-hydroxybutyrate-co-3-hydroxyvalerate) biocomposite coatings,EMRS 2014, Symposium : J Laser interaction with advanced materials: fundamentals and applications, Lille,France , May 26-30),Prezentare Poster, 27mai,cod panou: JP. VIII 40

11. A.S. Nikolov *, R.G. Nikov, N.N. Nedyalkov, P. A. Atanasov, M. T. Alexandrov, DKarashanova, N.E.Marinkov,I.Z.Dimitrov,I.IBoevski, **A.Visan** and I.Nmihailescu(2014) ,Influence of the liquid level and duration of the ablation process on the characteristics of nanostructures created by nanosecond laser ablation of Ag in water,EMRS 2014, Symposium : J Laser interaction with advanced materials: fundamentals and applications, Lille,France , May 26-30),Prezentare Poster

12. R. Cristescu, G. Dorcioman, C. Popescu, C. Nita, **A.Visan**, G. Socol, I.N. Mihailescu, D. Mihaiescu, A. Grumezescu, M. Enculescu, C. Chifiriuc, R. J. Narayan, and D. B. Chrisey(2014),,MICROBIAL COLONIZATION OF BIOPOLYMERIC THIN FILMS CONTAINING NATURAL COMPOUNDS AND ANTIBIOTICS FABRICATED BY MAPLE,EMRS 2014, Symposium : J Laser interaction with advanced materials: fundamentals and applications, Lille,France , May 26-30),Lectie invitata

13. **A.Visan**, A. C. Popescu, G. E. Stan, L. Duta, G. Dorcioman, O. Iordache, I. Dumitrescu, I. Pasuk, I. N. Mihailescu(2014),,ZnO and hydrophobin thin coatings on textiles substrates for biomedical applications,INERA WORKSHOP:Transition Metal Oxide Thin Films-functional Layers in “Smart windows” and Water Splitting devices: Technology and Optoelectronic properties ,September 4th – 6th, 2014,Varna, Bulgaria,Friday,Poster Session C: Novel thin film technologies and applications

14. **A.Visan**, A. C. Popescu, G. E. Stan, L. Duta, G. Dorcioman, O. Iordache, I. Dumitrescu, I. Pasuk, I. N. Mihailescu(2014),,ZnO and hydrophobin thin coatings on textiles substrates for biomedical applications,INERA WORKSHOP:Transition Metal Oxide Thin Films-functional

Layers in “Smart windows” and Water Splitting devices: Technology and Optoelectronic properties ,September 4th – 6th, 2014,Varna, Bulgaria,Prezentare oral

15. **A.Visan**, M. Miroiu, N. Stefan, C. Nita, G. Dorcioman, I. Zgura, O.L. Rasoga, C.S. Breazu, Iuliana Urzica, L. Sima , L.Ivan, A. Stanculescu, R. Cristescu, G. Socol, I.N. Mihailescu(2014),, Fabrication of embedded lysozyme into degradable polycaprolactone -polyethylene glycol coatings, E-MRS 2014 FALL MEETING September 15-19,Warsaw University of Technology,Poland, poster Symposium : E ,Biomimetics and regenerative medicine- EMRS FALL MEETING ,Varsovia,Polonia,poster E-3

16. G. Popescu-Pelin, E. Axente, F. Sima, I. Iordache, C. Nita, **A.Visan**, I. Zgura, O.L. Rasoaga, C.S. Breazu, A. Stanculescu, I.N. Mihailescu, G. Socol(2014),, Deposition of degradable polymeric coatings based on lysozyme embedded into poly(ε-caprolactone) /poly(lactic acid-co-glycolic acid) blends: a comparative study, E-MRS 2014 FALL MEETING,September 15-19,Warsaw University of Technology,Poland, poster Symposium : E Biomimetics and regenerative medicine EMRS FALL , MEETING 15 septembrie Varsovia,Polonia,poster E-2

17. **A.Visan**, Sanja Erakovic, Ana Jankovic, Carmen Ristoscu, Liviu Duta, Natalia Mihailescu, George Stan, Marcela Socol, Ovidiu Iordache, Iuliana Dumitrescu, Catalin Luculescu, Ion N Mihailescu, Dj. Janackovic and V. Miskovic-Stankovic(2014),, Pure and doped hydroxyapatite thin films synthesized by pulsed laser deposition for metal implant coatings, ISCP 2014, 23th – 26th September 2014, Orastie, Hunedoara, Prezentare Orala

18. **A.Visan**, Marimona Miroiu, Nicolae Stefan, Cristina Nita, Gabriela Dorcioman, Irina Zgura, Oana Rasoga, Carmen Breazu, Iuliana Urzica, Livia Sima, Luminita Ivan, Anca Stanculescu, Rodica Cristescu, Gabriel Socol and Ion N. Mihailescu(2014),, Embedded lysozyme into degradable polycaprolactone -polyethylene glycol coatings fabricated by Matrix Assisted Pulsed Laser Evaporation and Dip Coating Techniques, ISCP 2014, 23th – 26th September 2014, Orastie, Hunedoara,P26

19. G. Popescu-Pelin, E. Axente, F. Sima, I. Iordache, C. Nita, **A.Visan**, I. Zgura,O.L. Rasoga, C.S. Breazu, A. Stanculescu, G. Socol, I.N. Mihailescu(2014),, Polymeric coatings based on poly(ε-caprolactone)/poly(lactic acid-co-glycolic acid) deposited by MAPLE and dip-coating techniques: a comparative study, ISCP 2014, 23th – 26th September 2014, Orastie, Hunedoara,P22

20. N. Stefan, F. Miroiu, **A.Visan**, C. Nita, I. Zgura, O. Rasoga, R. Cristescu,G. Socol(2014), Fabrication of biodegradable silk fibroin - poly(sebacic acid) diacetoxy terminated composite coatings for local proteins release, ISCP 2014, 23th – 26th September 2014, Orastie, Hunedoara,P25

21. F. Miroiu, N. Stefan, **A.Visan**, C. Nita, R. Cristescu, I. Zgura, O. Rasoga,L. Sima,I. N. Mihailescu, G. Socol(2014),, Silk Fibroin – poly(3-hydroxybutyric-acid-co-3-hydroxyvaleric-acid composite biodegradable polymer coatings for biomedical applications, ISCP 2014, 23th

– 26th September 2014, Orastie, Hunedoara, P19

22. C. Nita, **A.Visan**, E. Axente, R. Cristescu, N. Stefan, M. Miroiu, G. Dorcioman,I. Zgura, O.L. Rasoga, C.S. Breazu, G. Socol(2014) , Comparative study of polycaprolactone and polylactic acid coatings-Physico, chemical and compositional investigations, ISCP 2014, 23th – 26th September 2014, Orastie, Hunedoara,P21

23. **A.Visan**, M. Miroiu, N. Stefan, C. Nita, G. Dorcioman,M.Socol, I. Zgura, O.L. Rasoga, C.S. Breazu, L. Sima , L.Ivan, A. Stanculescu, R. Cristescu, G. Socol, I.N. Mihailescu(2014), Encapsulated lysozyme into coatings of degradable polymeric blends fabricated by different methods, International Colloquium "Physics of Materials" Prezentare orala O3

24. **A.Visan**, S. Erakovic, A. Jankovic, C. Ristoscu, L. Duta, N. Mihailescu (Serban), G.E. Stan, M. Socol, O. Iordache , I. Dumitrescu, C.R. Luculescu,I.N. Mihailescu.Dj. Janackovic, V. Miskovic-Stankovic(2014), Fabrication and characterizations of pure and doped hydroxyapatite coatings for medical applications, International Colloquium "Physics of Materials", Prezentare poster P6, 14 noiembrie,Section 1 : Synthesis and characterization of Functional materials

25. Miroiu Floralice Marimona, Stefan Nicolaie, **A.Visan**, Nita Cristina, Cristescu Rodica, Zgura Irina, Rasoga Oana L., Mihailescu Ion N., Socol Gabriel(2014),Composite biodegradable biopolymer coatings of Silk Fibroin – Poly(3-Hydroxybutyric-acid-co-3-Hydroxyvaleric-acid) for biomedical applications", 10th International Conference on Physics of Advanced Materials (ICPAM-10), 22-28 septembrie 2014, Iasi, Romania, P10

26. **A.Visan**, Stefan Nicolaie, Miroiu Floralice Marimona, Nita Cristina, Dorcioman Gabriela, Zgura Irina, Rasoga Oana L., R, Breazu Carmen Steliana, Stanculescu Anca Ioana, Cristescu Rodica, Socol Gabriel, Mihailescu Ion N. (2014), „Comparative study on MAPLE and Dip Coating techniques for fabrication of biodegradable polymer thin films with medical applications", 10th International Conference on Physics of Advanced Materials (ICPAM-10), 22-28 septembrie 2014, Iasi, Romania, P11

27. Stefan Nicolaie, Miroiu Floralice Marimona, **A.Visan**, Nita Cristina, Zgura Irina, Rasoga Oana L., Stanculescu Anca Ioana, Socol Gabriel(2014), „Matrix Assisted Pulsed Laser Evaporation deposition of silk fibroin/poly(sebacic acid) diacetoxy terminated composite coatings for biodegradation medical applications", 10th International Conference on Physics of Advanced Materials (ICPAM-10), 22-28 septembrie 2014, Iasi, Romania, P12

28. A. Jankovic, N. Serban, L. Duta, S. Erakovi, C. Ristoscu, G.E. Stan, **A.Visan**, C. Luculescu, M.C. Chifiriuc, V. Miskovic-Stankovic, I.N. Mihailescu(2013); Pure and doped hydroxyapatite thin films synthesized by advanced laser techniques for metal implant coatings; Symposium V: Laser materials interactions for micro and nano applications of the E-MRS 2013 Spring Meeting, Congress Center in Strasbourg (France) from May 27 to 31, 2013;V.PI 35

29. S. Erakovic, A. Jankovic, C. Ristoscu, L. Duta, N. Serban, **A.Visan**, G. Stan, M. Socol, C.R. Luculescu, I.N. Mihailescu, V. Miskovic-Stankovic(2013); Pld Deposited Thin Films On

Titanium Modified By TiO_2 Nanotubes;Fourth Regional Symposium on Electrochemistry South East Europe (RSE-SEE), Ljubljana, 2013; 26 mai 2013,

30. **A.Visan**, D. Grossin, N. Stefan, L. Duta, F.M. Miroiu, M. Sopronyi, F. Miculescu, M. Freche, C. Charvilat, O, Marsan, S. Ciuca, I.N. Mihailescu(2013) "; Biomimetic nanocrystalline apatite coatings synthesized by Matrix Assisted Pulsed Laser Evaporation for medical applications"; Conferinta Internationala "Modern Laser Applications (INDLAS)", a 3-a Editie, Bran, Romania, 20-24 Mai 2013, P29

31. **A.Visan**, D. Grossin, N. Stefan, L. Duta, F. M. Miroiu, M. Sopronyi, F. Miculescu, M. Freche, C. Charvilat, O, Marsan, S. Ciuca, I.N. Mihailescu(2013) ; "Biomimetic nanocrystalline apatite coatings synthesized by Matrix Assisted Pulsed Laser Evaporation for medical applications";„13-th International Balkan Workshop on Applied Physics and Materials Science (IBWAP)", Constanta, Romania, 4-6 Iulie 2013; S4 P13.

32. **A.Visan**, D. Grossin, N. Stefan, L. Duta, F. M. Miroiu, M. Sopronyi, F. Miculescu, M. Freche, C. Charvilat, O. Marsan, S. Ciuca, I. N. Mihailescu(2013) ; "Biomimetic nanocrystalline apatite coatings synthesized by matrix assisted pulsed laser evaporation for medical applications"/orala; „10-th International Student Conference of the Balkan Physical Union (ISCBPU)", Universitatea din Istanbul, Facultatea de Stiinte, Istanbul, Turcia, 3-5 Septembrie 2013; 4 septembrie 2013

33. **A.Visan**, D. Grossin, N. Stefan, L. Duta, F. M. Miroiu, M. Sopronyi, F. Miculescu, M. Freche, C. Charvilat, O, Marsan, S. Ciuca, I.N. Mihailescu(2013) ;"Biomimetic nanocrystalline apatite coatings synthesized by Matrix Assisted Pulsed Laser Evaporation for medical applications"/orala; „25-th Symposium and Annual Meeting of the International Society for Ceramics in Medicine (Bioceramics 25)", Bucuresti, Romania, 07-10 Noiembrie 2013; 8 noiembrie 2013; O.4.6

34. A. Jankovic, N. Serban, L. Duta, S. Erakovic, C. Ristoscu, G.E. Stan, **A.Visan**, C. Luculescu, M.C. Chifiriuc, V. Miskovic-Stankovic, I.N. Mihailescu(2013) ;"Pure and doped hydroxyapatite thin films synthesized by advanced laser techniques for metal implant coatings";Oral presentation; „25-th Symposium and Annual Meeting of the International Society for Ceramics in Medicine (Bioceramics 25)", Bucuresti, Romania, 07-10 Noiembrie 2013; 8 noiembrie 2013; O.4.7.

35. C. Nita, E. Axente, **A.Visan**, F. Sima, V. Grumezescu, C. Breazu, O. Rasoga, M. Socol, I. Zgura, L. E. Sima, G. Chiritoiu, and G. Socol(2013); Kinetic release of Lysozyme embedded in biodegradable PCL/PLA composite coatings-prezentare orala; 10th International Student Conference of the Balkan Physical Union, Istanbul, Turcia, 3-5 septembrie 2013; 4 septembrie 2013;

36. **A.Visan**, M. Miroiu, C. Nita, R. Cristescu, G. Socol, N. Stefan, G. Dorcioman, N. Serban, M. Socol, I.Zgura, O.L. Rasoga, C. Breazu, L. Sima, C. R. Luculescu, A. Stanculescu, I.N. Mihailescu(2013) ; Characteristics and biodegradation properties of polycaprolactone - polyethylene glycol coatings for tissue engineering applications Prezentare poster; The 13th

International Balkan Workshop on Applied Physics and Materials Science Constanta, Romania, 4-6July 2013; S4 P12.

37. **A.Visan**, M. Miroiu, C. Nita, R. Cristescu,G. Socol, N. Stefan, F.Sima, G. Dorcioman, N. Serban, , M. Socol, L. Sima, C. R. Luculescu , A. Stanculescu, I.N. Mihailescu(2013) ; Characteristics and biodegradation properties of polycaprolactone -polyethylene glycol coatings for tissue engineering applications; Conferinta Internationala "Modern Laser Applications (INDLAS)", a 3-a Editie, Bran, Romania, 20-24 Mai 2013, P 30.

38. **A.Visan**, M. Miroiu, R. Cristescu,G. Socol, N. Stefan, G. Dorcioman, F Sima, C. Nita, M. Socol, L. Sima, C. R. Luculescu, A. Stanculescu, I.N. Mihailescu(2013); Characteristics And Biodegradation Properties Of Polycaprolactone -Polyethylene Glycol Coatings For Tissue Engineering Applications;Prezentare Poster; E-MRS 2013 SPRING MEETING Congress Center - Strasbourg, France,May 28-30; V P II 20

39. N. Stefan, FM. Miroiu, R. Cristescu, **A.Visan**, V. Grumezescu, C. Nita, M. Socol, O. Rasoga, L. Sima, IN Mihailescu, G. Socol(2013) ; Fabrication Of Biodegradable Silk Fibroin - Poly(Sebacic Acid) Diacetoxy Terminated Composite Coatings For Local Release Of Proteins;Prezentare Poster; E-MRS 2013 SPRING MEETING, Congress Center - Strasbourg, France,May 28-30; V P II 9.

40. F. Miroiu, G. Socol, N. Stefan , **A.Visan**, C. Nita, R. Cristescu, F. Sima, V. Grumezescu, M. Socol, I. Zgura, O. Rasoga, L. Sima, I. N. Mihailescu(2013); Silk Fibroin – Based Composite Biodegradable Polymer Coatings For Biomedical Applications;Prezentare Poster; E-Mrs 2013 Spring Meeting Congress Center - Strasbourg, France,May 28-30; V P II -21.

41. F. Miroiu, G. Socol, N. Stefan, **A.Visan**, C. Nita, R. Cristescu, F. Sima, V. Grumezescu, M. Socol, I. Zgura, O. Rasoga, L. Sima, I. N. Mihailescu;Silk Fibroin – Based Composite Biodegradable Polymer Coatings For Biomedical Applications;Prezentare orala; 10th International Student Conference of the Balkan Physical Union; 4 septembrie 2013; 18:00-18:15.

42. N. Stefan, FM. Miroiu, R. Cristescu, **A.Visan**, V. Grumezescu, C. Nita, M. Socol, O. Rasoga, L. Sima, IN Mihailescu, G. Socol ; Fabrication Of Biodegradable Silk Fibroin - Poly(Sebacic Acid) Diacetoxy Terminated Composite Coatings For Local Release Of Proteins;Prezentare Poster; 10th International Student Conference of the Balkan Physical Union; PP-21-SON.

43. S. Eraković, A. Janković, C. Ristoscu, L. Duta, N. Serban, **A.Visan**, I.N. Mihailescu, G.E. Stan, M. Socol, O. Iordache, I. Dimitrescu, C.R. Luculescu, Dj. Janaćković, V. Mišković-Stanković(2013) ; Silver/hydroxyapatite coating on pure and anodized titanium obtained by pulsed laser deposition; YUCOMAT 2013, Herceg Novi, 2013, Montenegro; P S E 12, pg 50

44. Sanja Eraković, Ana Janković, Carmen Ristoscu, Liviu Duta, Natalia Serban, **A.Visan**, George E. Stan, Catalin Luculescu, Djordje Janacković, Ion N. Mihailescu, Vesna Mišković-Stanković (2013);Laser assembling of thin bioceramic and biocomposite films on titanium utilizing Pulsed laser deposition (PLC) and Matrix-assisted pulsed laser evaporation (MAPLE) techniques; Twelfth Young Researchers' Conference-Materials Science and Engineering, 2013, Belgrade, Serbia; 13 decembrie 2013; X II / 1; pg 41. 16:30-16:45

45. F. Miroiu, G. Socol, N. Stefan , **A.Visan**, C. Nita, R. Cristescu, F. Sima, V. Grumezescu, M. Socol, I. Zgura, O. Rasoga, L. Sima, I. N. Mihailescu(2013); silk fibroin – based composite biodegradable polymer coatings for biomedical applications;Prezentare Poster; Conferinta Internationala "Modern Laser Applications (INDLAS)", a 3-a Editie, Bran, Romania, 20-24 Mai 2013, P35

AIS=3,385 ; Factor ISI = 1,086 ; h=3 ; 29 citations